JOURNAL OF GEOPHYSICAL RESEARCH, VOL. 105, NO. D8, PAGES 10,023–10,045, APRIL 27, 2000

An overview of the Stratospheric-Tropospheric Experiment: Radiation, Aerosols, and Ozone (STERAO)-Deep Convection experiment with results for the July 10, 1996 storm

J.E. Dye,[1] B.A. Ridley,[1] W. Skamarock,[1] M. Barth,[1] M.Venticinque,[1]
E. Defer,[2] P. Blanchet,[2] C. Thery,[2] P. Laroche,[2] K. Baumann,[1,7]
G. Hubler,[3] D.D. Parrish,[3] T. Ryerson,[3] M. Trainer,[3] G. Frost,[3] J.S. Holloway,[3]
T. Matejka,[4] D. Bartels,[4] F.C.Fehsenfeld,[3] A. Tuck,[3]
S. A. Rutledge,[5] T. Lang,[5] J. Stith,[6] and R. Zerr[6]

Abstract. The Stratospheric-Tropospheric Experiment: Radiation, Aerosols and Ozone (STERAO)-Deep Convection Field Project with closely coordinated chemical, dynamical, electrical, and microphysical observations was conducted in northeastern Colorado during June and July of 1996 to investigate the production of NO_X by lightning, the transport and redistribution of chemical species in the troposphere by thunderstorms, and the temporal evolution of intracloud and cloud-to-ground lightning for evolving storms on the Colorado high plains. Major observations were airborne chemical measurements in the boundary layer, middle and upper troposphere, and thunderstorm anvils; airborne and ground-based Doppler radar measurements; measurement of both intracloud (IC) and cloud-to-ground (CG) lightning flash rates and locations; and multiparameter radar and in situ observations of microphysical structure. Cloud and mesoscale models are being used to synthesize and extend the observations. Herein we present an overview of the project and selected results for an isolated, severe storm that occurred on July 10. Time histories of reflectivity structure, IC and CG lightning flash rates, and chemical measurements in the boundary layer and in the anvil are presented showing large spatial and temporal variations. The observations for one period of time suggest that limited mixing of environmental air into the updraft core occurred during transport from cloud base to the anvil adjacent to the storm core. We deduce that the most likely contribution of lightning to the total NO_X observed in the anvil is 60-90% with a minimum of 45%. For the July 10 storm the NO_X produced by lightning was almost exclusively from IC flashes with a ratio of IC to total flashes >0.95 throughout most of the storm's lifetime. It is argued that in this storm and probably others, IC flashes can be major contributors to NO_X production. Superposition of VHF lightning source locations on Doppler retrieved air motion fields for one 5 min time period shows that lightning activity occurred primarily in moderate updrafts and weak downdrafts with little excursion into the main downdraft. This may have important implications for the vertical redistribution of NO_X resulting from lightning production, if found to be true at other times and in other storms.

[1]National Center for Atmospheric Research, Boulder, Colorado
[2]Office Nationale d'Etudes et de Recherché Aerospatiales, Chattilon, France
[3]NOAA Aeronomy Laboratory, Boulder, Colorado
[4]NOAA National Severe Storms Laboratory, Boulder, Colorado
[5]Department of Atmospheric Sciences, Colorado State University, Fort Collins, Colorado
[6]Department of Atmospheric Sciences, University of North Dakota, Grand Forks, North Dakota
[7]Now at School of Earth and Atmospheric Science, Georgia Institute of Technology, Atlanta, Georgia

Paper number 1999JD 901116.
0148-0227/00/1999JD01116$09.00

1. Introduction

It is widely recognized that thunderstorms play a major role in both weather and climate through important chemical, dynamical, electrical, and radiative processes. However, because of the complexity of these interactive processes, few projects have been undertaken to try to quantify this role. To properly address these interdependent scientific problems requires highly focused, closely coordinated measurements from several disciplines of atmospheric science.

The Stratospheric-Tropospheric Experiment: Radiation, Aerosols, and Ozone (STERAO) series of projects was initiated to address these important problems. STERAO-A (Deep Convection and the Composition of the Upper

Troposphere and Lower Stratosphere) was the first of three projects that was to be followed by two others: one on aerosols and cirrus cloud properties and another on photochemistry of the near-tropopause region. A main objective of STERAO-Deep Convection is to determine the effects of thunderstorms on the chemical structure of the middle and upper troposphere, particularly the production of NO_X (= NO + NO_2) by lightning and transport of NO_X from the boundary layer. Subsequent effects on ozone will be investigated in modeling studies. Another goal of the project is to relate the frequency and location of both intracloud and cloud-to-ground lightning to evolving reflectivity and airflow structure for storms of the Colorado high plains. This goal is important in its own right for understanding storm behavior and possible nowcasting applications, but also is a critical component for the studies of NO_X production by lightning.

STERAO-Deep Convection (henceforth simply referred to as STERAO) was successful in combining detailed chemical, electrical, kinematic, and microphysical measurements around thunderstorms and in thunderstorm anvils. STERAO provided information on the transport of chemical constituents from the boundary layer into the upper troposphere, the production of NO_X by lightning, the lightning characteristics of evolving storms of the high plains, and some limited information on stratospheric-tropospheric exchange. Section 2 describes the design of the experiment and the measurement systems and platforms used in the project. Section 3 presents observations for a storm studied on July 10 as an example of results obtained during STERAO. Section 4 provides concluding remarks on issues and future projects, which are being and can be addressed with the STERAO - Deep Convection data set.

2. Project Description

2.1. Facilities and Operational Area

The major facility components of the project described in the following subsections were (1) the Colorado State University (CSU) CHILL's multiparameter Doppler radar, to observe the evolving storm structure; (2) a National Oceanic and Atmospheric Administration (NOAA) WP3D Orion aircraft, to characterize the chemical environment in which storms were growing, to determine the concentrations of constituents entering or exiting the storm in the boundary layer and midcloud levels, and to obtain Doppler radar measurements for deducing storm airflow patterns; (3) the University of North Dakota Citation jet aircraft, to make chemical, airflow, and microphysical measurements in and around the anvils of the storms; (4) the French Office Nationale d'Etudes et de Recherches Aerospatiales (ONERA) three dimensional (3-D) lightning interferometer, to determine total lightning flash rates and map lightning channels in the storms; (5) the National Lightning Detection Network (NLDN), to determine times and locations of cloud-to-ground lightning; and (6) the National Center for Atmospheric Research (NCAR) Atmospheric Technology Division mobile Cross-Chain Loran Atmospheric Sounding System (CLASS) for environmental soundings. A map of the operational area and location of facilities is shown in Figure 1. The operations center for the project was located in the radar control van at the CSU-CHILL radar site.

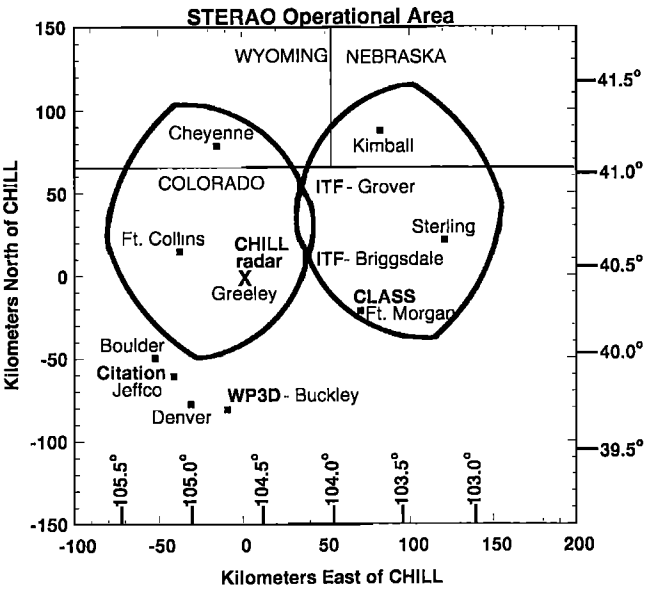

Figure 1. The STERAO operational area in northeastern Colorado, showing locations of ground facilities and the lightning interferometer lobes. Longitudes and latitudes are shown along the bottom and right side of the figure.

The field experiment was conducted in northeastern Colorado during the summer of 1996 with aircraft observations concentrated in a 4 week period from mid-June to mid-July. Colorado was chosen because there is a high frequency of storms in the area ranging from simple air mass to multicell, to supercell thunderstorms, because it is close to Denver with suitable locations for aircraft operation; and because the CSU - CHILL radar is located in the area near Greeley. During the 4 week period when aircraft were available, measurements were obtained in 14 storms with either one or both aircraft. See Table 1 for a list of flights with brief comments on each storm. The project also collected combined radar and lightning data daily from mid-June to early September, thus providing measurements on both intracloud (IC) and cloud-to-ground (CG) lightning for a wide variety of storm types of the central high plains.

2.2. Project Design

A climatological study of storms of northeastern Colorado during the National Hail Research Experiment (1972 -1976) showed a maximum frequency of occurrence around 1500 LT (2100 UTC) [*Fankhauser and Wade*, 1982], so our operations were keyed to this approximate time. Daily weather briefings were held at 0900 LT in Boulder using facilities and forecast outputs of the NOAA Forecasting Systems Laboratory (FSL) and given by FSL or NOAA National Severe Storms Lab (NSSL) personnel. Additionally, the NCAR MM5 real-time model and the NASA Goddard/University of Maryland/State University of New York at Brockport 2-D cumulus ensemble model were used for guidance. Plans were made each morning for anticipated takeoffs of the WP3D and Citation based on the forecast for deep convection coupled with a sense of previous climatology. Actual takeoffs were sometimes delayed when convective activity developed later than expected.

Table 1. STERAO Cases With Aircraft Observations

Date	P3	Citation	Comments
June 17	1507 - 2214	...	SW tail of distant squall line
June 22	1409 - 2055	...	narrow line along foothills
June 26	...	1717 - 2020	active storm West of Fort Collins
June 27	1404 - 1817	1510 - 1830	small, air mass Cb
June 28	1409 - 1826	1620 - 1830	remnants of squall line
June 29	1402 - 1801	1410 - 1545	intercomparison flight
July 5	...	1450 - 1800	anvil passes in storm East of area
July 6	1503 - 1816	...	weak, short-lived thunderstorms
July 7	1537 - 1907	...	small, short-lived thunderstorms
9 July	1529 - 2106	1410 - 1600	embedded multicells changing
		1715 - 2010	to large stratiform
10 July	1535 - 2025	1610 - 1930	multicell evolving to supercell
12 July	1434 - 2126	1620 - 1925	multicell evolving to intense cell
13 July	1458 - 2021	1510 - 1800	numerous strong cells
15 July	...	1616 - 1845	spiral in lower upshear anvil
16 July	1156 - ⇒	1157 - 1415	intercomparison flight; Tampa return
16 July	...	1550 - 1810	moderate storm, spirals in and downwind of anvil

All times are mountain daylight time; add 6 hours for UTC.

The WP3D with an endurance of >8 hours normally took off about 1300 LT, a couple of hours before storms were anticipated, to map the chemical, thermodynamic, and dynamic prestorm environment in the operational area. This consisted of flying roughly 100 km long north-south and then west-east flight legs starting at 150 to 200 m above the surface (~1700 m mean sea level (msl)). These were followed by a continuous vertical spiral to about 7000 m msl and a stepped downward profile. When storms did form, the WP3D was directed to the storm selected by the operations director at the operations center at CHILL. After the WP3D proceeded to the selected storm, it was flown about 15 to 20 km from and parallel to the long axis of the storm in a manner such that profiles of chemical constituents and Doppler radar measurements could both be obtained. The legs were incremented in altitude from near the surface to 7 - 8 km msl.

When a storm was selected, the Citation (which has an endurance of about 3 ½ hours and a ceiling of roughly 12.5 km) was directed to take off and proceed to the anvil of the storm of interest. The ascent in route to the storm and descent upon return to base provided important vertical soundings of the environment and often were representative of the undisturbed environment. Complete soundings near the storms were not made because of the limited endurance of the aircraft. Upon reaching the storm the Citation made successive penetrations of the anvil incremented up or down in altitude. When possible, vertical spirals were made through the visible extent of the anvil.

Radio communications to each aircraft were maintained from the CHILL operations near Greeley (Figure 1). Radar images, weather and satellite images, and real-time 2-D plots of total lightning activity from the ONERA lightning interferometer were all displayed in the operations center. Aircraft positions transmitted via phone line from the Federal Aviation Administration (FAA) were overlaid on the CHILL radar PPIs (plan position indicator sweeps). Thus the operations director could identify and monitor storm location, motion, structure, and evolution, the presence of lightning within the storm, and locations of the aircraft relative to the storm and lightning. The real-time total lightning information from the interferometer proved to be particularly interesting because it identified new regions of active convection before the regions became clearly recognizable on radar.

2.3. Radar Observations

The CSU-CHILL 11 cm radar provided multiparameter Doppler radar observations for both real-time operations and postproject analysis. The operating characteristics of the radar are listed in Table 2. The reflectivity measurements provide the main source of information on the evolution of storms and allow us to relate the lightning and airborne chemical measurements to the storm structure and evolution. Sphere, solar, and daily receiver calibrations performed during the experiment suggest uncertainty in the reflectivity measurements of ± 1 dBZ. The CHILL Doppler measurements supplement the airborne Doppler measurements made from the WP3D discussed below. The multiparameter measurements of differential reflectivity

Table 2. CSU - CHILL Radar Characteristics

Parameter	Value
Antenna (parabolic)	
Diameter	8.5 m
Half-power beam width	1.1°
Gain	45 dB
First side lobe	-27 dB
Polarization	
Transmit	horizontal and vertical
Receive	horizontal and vertical
Cross-pole isolation	-35 dB
Transmitter (dual)	
Wavelength	11.01 cm
Peak power	1 MW
Pulse length	1.0 μs
Pulse repetition time	800 - 200 ms
Receiver (dual)	
Dynamic range	> 85 dB
Minimum detectable signal	-115 dBm
Variables[1]	Vr, Z_h, Z_{DR}, Φdp, LDR, ρ^*
Range	75 km with 150 m gates or 150 km with 300 m gates

[1] velocity, reflectivity, differential reflectivity, differential phase, linear depolarization ratio, copolar correlation

Table 3. NOAA WP3D Tail Radar Characteristics With French CNRS Atenna

Parameter	Value
Wavelength	3.22 cm
Peak power	60.0 kW
Pulse length	0.5 μs
Pulse repetition period	625 μs
Maximum unambiguous range	92.6 km
Maximum unambiguous velocity	12.9 m/s
Half-power beam width	
Fore, horizontal	2.02°
Fore, vertical	2.03°
Aft, horizontal	2.02°
Aft, vertical	2.05°
Gain	
Fore	37.9 dB
Aft	37.5 dB
Polarization	
Transmit	horizontal
Receive	horizontal
Tilt angle	
Fore	19.8°
Alt	-19.9°
Minimum detectable signal	-111 dBm

CNRS denotes Centre National de la Recherche Scientifique.

(Z_{DR}), differential phase (φdp), linear depolarization ratio (LDR), and copolar correlation (ρ^*) are used to identify regions containing large raindrops, graupel, and hail and yield information on rainfall and hail fluxes from the storms. These measurements are important for validating model simulations of storms. A review of multiparameter measurements and their application is given by *Doviak and Zrnic* [1993]. The radar was normally scanned by incrementing sector sweeps from a low elevation angle to above radar storm top to try to complete volume scans of the entire storm within 5 to 6 min. A low-level 360° sweep taken between sector scans to monitor convection over the entire area. Occasional vertical cross sections (range-height indicators, (RHIs)) were taken in regions of interest.

The WP3D scanning X band (3 cm) Doppler tail radar, operated in STERAO by personnel of NOAA/NSSL, was the main source of measurements for determining airflow fields within the storms. Operating characteristics of this radar are given in Table 3. The fore-aft scanning technique (FAST) [*Jorgensen et al.*, 1996], which makes rotating sweeps alternating at angles of about 20° fore and aft of a plane perpendicular to the aircraft track, was used to gather Doppler radar measurements. This permits reconstruction of the airflow field from a single pass of the aircraft along the length of the storm. The flight pattern gave volume scans approximately every 10 min. Postproject analysis, which includes combination of the airborne Doppler measurements with the CHILL ground-based measurements, shows that high-quality measurements were collected. The WP3D also has a C band lower fuselage radar to provide surveillance coverage of storms in the area.

2.4. Airborne Chemistry Measurements

The chemical instrumentation of the WP3D was coordinated by the NOAA Aeronomy Lab and included

Table 4: Instrumentation on the NOAA WP3D

Parameter/Species	Method	Uncertainty
NO	NO/O^3	30 pptv + 15% (1 s)
O^3	UV absorption and NO/O^3 chemiluminescence	30 ppbv + 3% (1 s)
CO	UV resonance fluorescence	3 ppbv + 3% (1s)
SO^2	UV resonance fluorescence	
C^2-C^5 VOC	in situ gas chromatography/ flame ionization detection	
NMHC canister	postflight gas chromatography/ flame ionization detection	
PAN, PPN, and $RONO^2$	gas chromatography/ electron capture detector	
Total peroxide	scrubbing into solution, enzyme reaction, fluorescence detection	
Formaldehyde	tunable diode laser absorption spectrometer	
Water vapor	Lyman alpha absorption	
UV fluxes	UV radiometer (300-400 nm) zenith and nadir	
Aerosol number	Condensation nuclei counter: saturation chamber	
Aerosol light scatter	multiwavelength nephelometer	
Aerosol light absorption	aethalometer	
Particle size		
Distributions	PMS forward scattering spectrometer Probe (1-45 μm)	
	PMS 2-D grey cloud probe (25-1600 μm)	
State parameters	Standard techniques	
u,v,w winds	Inertia navigation	
Aircraft position	GPS receiver	
Reflectivity field	C and X band radar	

NMHC denotes nonmethane hydrocarbons; PAN denotes peroxyacetylnitrate; PPN denotes peroxyproprionyl intrate; $RONO^2$ denotes alkyl nitrates and PMS denotes Particle Measuring Systems.

Table 5. Instrumentation on the UND Citation

Parameter	Method	Uncertainty
NO	chemiluminescence	12pptv + 5% (1 s)
O_3	scintrex	±10% (1 s)
CO	IR absorption	±20% (20 s)
Water vapor	cryogenic frost point	
Hydrocarbons	whole air sampler	
Particle size distributions	PMS forward scattering spectrometer probe (1-45 μm	
	PMS 2-D cloud probe (25-800 μm)	
	PMS 1-D precipitation probe (0.2-6.4 mm)	
	PMS active scattering aerosol spectrometer probe (0.3-5 μm)	
State parameters	standard techniques	
u, *v*, *w*, winds	inertial navigation	
Aircraft position	GPS and INS	

GPS denotes Global Positioning System, and INS denotes inertial navigation system.

instruments from the Aeronomy Lab, NOAA Climate Monitoring and Diagnostics Lab, and NCAR. A list of the measurements available from STERAO, the measurement techniques, and estimated measurement uncertainty for instruments used in the present study are shown in Table 4. The primary chemical constituents for STERAO were NO, ozone, CO, hydrocarbons, formaldehyde, peroxide, and water vapor. Ozone, CO, and hydrocarbons are useful as tracers of air mass transport. Signals for most of the instruments were recorded at 1 Hz, which gives spatial resolution of 100 to 120 m at the typical air speed of the WP3D. For hydrocarbons, 5 min integrated in situ, real-time gas chromatograph samples were taken continuously, and canister grab samples varying in length from 20 to 60 s were taken at selected times for later analysis. Additionally, the state parameters of temperature, pressure, radar altitude, true air speed, aircraft position, heading, attitude, and horizontal and vertical air motions were measured using the standard NOAA Aircraft Operations Center instrument package. The Particle Measuring Systems, 2-D gray scale probe was used to observe precipitation particles and the FSSP 100 for cloud droplets, although the WP3D normally flew outside of cloud and away from cloud and precipitation.

The parameters measured on the Citation, measurement techniques, and estimated uncertainties for primary instruments are shown in Table 5. Payload capability necessarily limited the number of chemical constituents, which could be measured. Measurements included NO, ozone, condensation nuclei (CN), and alternately either CO or whole air canisters to sample hydrocarbons and other trace species. Postproject analysis showed that for unknown reasons the CN instrument often did not function properly above 6 or 7 km. The CO instrument was a highly modified commercial instrument that had an effective response time of greater than 20 s because available power limited the size of the pump that could be used. A description of the CO instrument, along with calibration procedures and corrections to the measurements, is provided in Appendix A. The Citation also carries a large complement of microphysical instruments shown in Table 5.

2.5. Intercomparison Flights

Two intercomparison flights were made with the WP3D and Citation to compare chemical, thermodynamic, and wind measurements. Side-by-side legs were flown from 2000 to 5000 m msl (500 to 3500 m above ground level); thus no comparisons are available for higher altitudes, low humidities, and temperatures colder than ≈-5°C. Temperatures agreed to within 0.1°C, dew point temperatures to within 0.5°C, and horizontal winds to within 1 m s^{-1}. Ozone measurements on the two aircraft were well correlated but showed an offset with the Citation about 5 ppbv higher. This offset has not been taken into account in the measurements presented below. The intercomparison flights revealed an initial discrepancy between the NO measurements on the WP3D and the Citation. However, after recalibration of flow controllers on the WP3D instrument, the NO measurements from the intercomparison flights agreed to within the uncertainty given for both instruments in Tables 4 and 5. For CO the intercomparison flights showed the Citation values to be on average 17% higher than on the P3. Consequently, the Citation CO data for all days were reduced by 17% to bring the archived data set of the Citation and WP3D as a whole into agreement. Additionally, a correction factor of 1.20 was made to the Citation CO data for July 10 because of erratic behavior of the in-flight sensitivity calibrations for that day. See Appendix A for discussion of these corrections.

2.6. Lightning Measurements

An important component of the STERAO project was the ability to detect both intracloud (IC) and cloud-to-ground (CG) flashes. The total lightning flash rates, flash durations, and VHF emission source locations along the lightning channels were determined using the ONERA lightning interferometer system [*Laroche et al.* 1994]. The CG flash rates and ground strike locations were monitored using the National Lightning Detection Network (NLDN). The ONERA interferometer is a 3-D system which can provide a map of lightning flashes with information on time, location, shape, and type of lightning for flashes suitably positioned. [*Laroche et al.* 1994; also E. Defer et al., Lightning activity of the July 10, 1996 storm during the Stratospheric-Tropospheric Experiment: Radiation, Aerosols, and Ozone Experiment submitted to *Journal of Geophysical Research*, 1999 (hereinafter Defer et al., submitted manuscript, 1999)]. Detection efficiency of flashes within the two lobes (Figure 1) is thought to be very nearly 100%. Information on the 3-D position of VHF radiation emission sources from lightning discharge

channels is recorded at each of the two antenna sites for postproject analysis, and 2-D horizontal (x,y) positions are displayed in real time. The real-time measurements were displayed in the operations center at CHILL and were very useful for identifying the progression of lightning activity, identifying areas of new growth, selecting storms for study, and guiding aircraft. See Appendix B for additional discussion of the different components of a lightning flash, the interferometer measurements and uncertainties, and the space and time criteria used to identify individual flashes.

The National Lightning Detection Network (NLDN) determines the time, ground strike location, polarity, maximum current, and number of CG flashes and strokes. This information was obtained through collaboration with NASA Marshall Space Flight Center. The NLDN system as configured in 1996 is reported to detect 90% of CG flashes in NE Colorado and to have median location accuracies of 500 m [*Cummins et al.*, 1998]. However, using a new technique for detecting negative CG flashes with the ONERA interferometer, Defer et al. (submitted manuscript, 1999) suggested that for negative CG lightning occurring during the July 10 storm the NLDN detection efficiency approached 100%. In this paper we use the NLDN measurements for determination of CG flash rates and the interferometer for total flash rates, and we subtract the CG flash rates from the total flash rates to determine IC flash rates. We estimate the uncertainty of total and IC flash rates to be <5%.

In addition to the NLDN and interferometer, students from CSU deployed two fixed field change meters and one mobile field change meter designed and built at New Mexico Tech. The field change meters (sometimes referred to as slow antennas) detect changes in the electrostatic electric field and are range sensitive. Nominally, the field change meters we used can detect both IC and CG lightning within 35 to 40 km of the sensor, but detection is dependent upon the strength of the discharge as well as distance. They are unable to distinguish direction to the flash. Hence if more than one storm or cell is present, there is ambiguity as to which storm (cell) produced the flash. The two fixed meters were located at the CHILL radar site and at Fort Morgan airport (Figure 1). The mobile field change meter was often directed to intercept individual storms. *Lang* [1997] provided a discussion of the slow antenna measurements and a comparison of some results with the interferometer.

2.7. Environmental Soundings

Environmental soundings for prediction and for postprogram modeling were made using the mobile CLASS sounding system from the NCAR Surface Soundings System Facility. Sondes were released from the Fort Morgan airport, which is near the middle of the operational area, at 0800 LT (1400 UTC) daily and between 1400 to 1500 LT (2000 to 2100 UTC) on days for which deep convection was anticipated. Measurements included temperature, pressure, relative humidity, and position from which horizontal winds can be determined. Ascents and descents of the aircraft, particularly the WP3D, which frequently was ascending or descending through the boundary layer and into the midtroposphere in the vicinity of the storms, provide important supplements to the balloon soundings, as does the Citation in the upper troposphere.

3. An Example From STERAO: The Storm of July 10, 1996

Observations made during the storm of July 10 provide examples of measurements collected during STERAO and some results from the project. The July 10 storm was a very isolated storm with no other storms within at least 150 km. The convection began northwest of Kimball, Nebraska, at about 2100 UTC (1500 LT) as isolated clouds which grew and decayed. By approximately 2130, two small cells oriented in a NW to SE direction along a confluence line persisted and ultimately matured into the storm studied here. The first lightning (an IC flash) occurred in the storm at 2152 UTC. During the first few hours of its lifetime (until about 0100 UTC (1900 LT)), the storm had a multicellular structure with new cells forming to the NW along the confluence line. In its later stage of development beginning near 0115, it evolved into a unicellar storm before decaying at ~0245. Observers on the ground and aboard the WP3D reported that the storm had cyclonic rotation at lower levels and a weak echo region and lacked a well-developed precipitation shaft. All of these features are characteristics of a low-precipitation (LP) supercell and observers near the storm (H. Bluestein, M. Weisman, and A. Seimon, personal communications, 1997) considered it a LP supercell in its later stages, although supercells normally are longer lived.

The cloud base temperature was approximately 7° to 7.5° C at an altitude of 3.6 to 3.7 km msl as determined from WP3D on-board video and temperature measurements. All altitudes herein are in km above mean sea level (msl) unless otherwise noted. Local terrain is at nominally 1.5 km msl. Thermodynamic and wind soundings constructed from the CLASS sounding at Fort Morgan and the WP3D are described in the paper by [*Skamarock et al.* 2000]. *Lang et al.* [2000] presented multiparameter estimates of hail fall and rainfall that show that the rainfall from the July 10 storm was much less in comparison to another excellent STERAO case, July 12. A photograph (Figure 2) taken by Anton Seimon from the WP3D on the SW flank of the storm during the supercell stage shows the well-developed upshear anvil, the overshooting top, and some precipitation. Views of the visible channel of the GOES 8 satellite at three different times during the storm history are presented by [*Skamarock et al.* 2000].

3.1. Radar Evolution and Structure

Constant altitude radar sections (CAPPIs) of the storm taken near cloud base at 4.5 km msl at intervals of roughly 1 hour are shown in Figures 3a-3d. These were constructed from interpolated, gridded data using the CEDRIC software developed by *Mohr et al.* [1986]. The first lightning occurred about 17 min prior to Figure 3a at 2152 UTC (hereafter times will be given in UTC, which is 6 hours ahead of local time, mountain daylight time). The most intense multicellular phase is represented in Figure 3b and the supercellular stage in Figure 3d. Flight tracks of the WP3D are superimposed on the radar contours illustrating the flight legs that served both Doppler and chemical measurements. Although elongated in the NW-SE direction, cells were at times only 15 – 20 km across in the SW to NE direction at cloud base. Figures 4a-4d depict the reflectivity structure at 10.5 km, showing the anvil

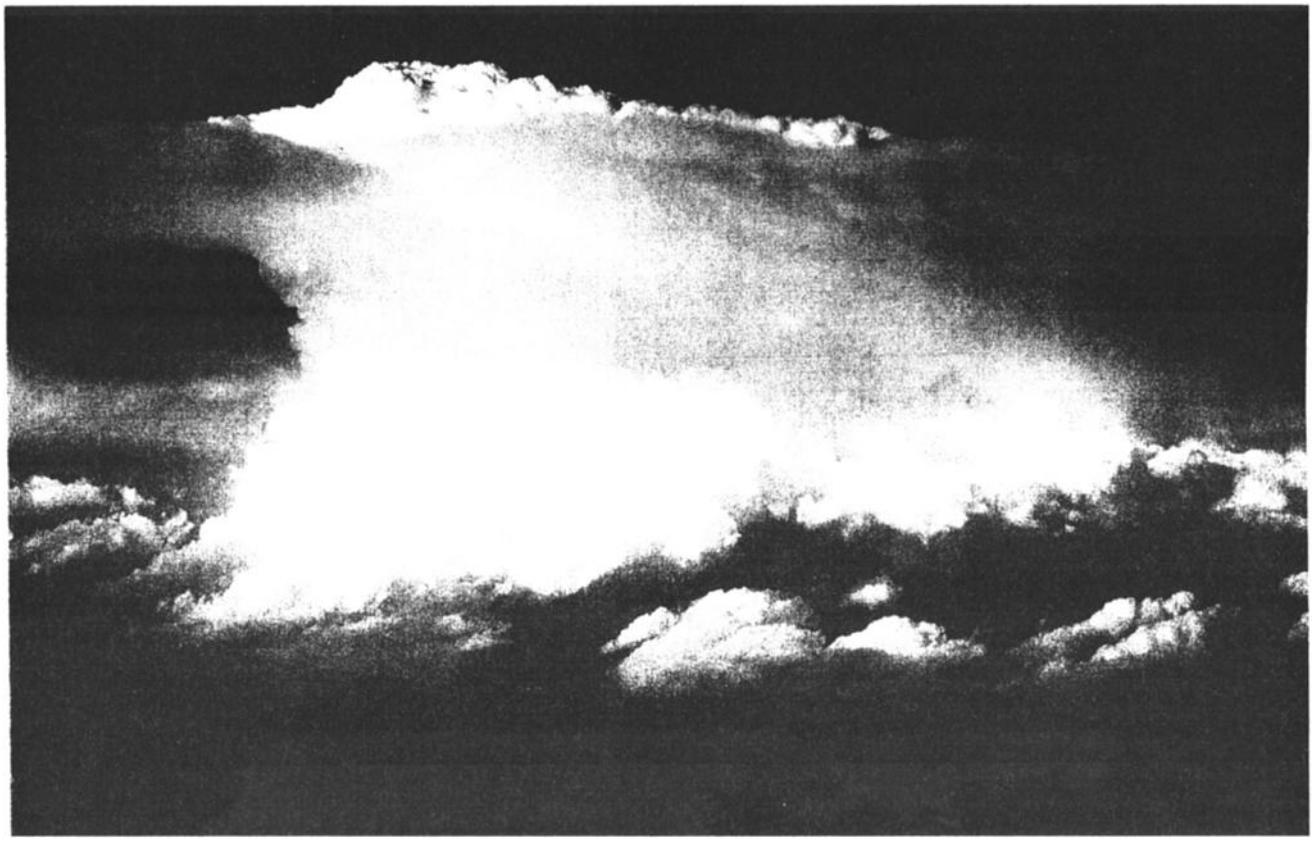

Figure 2. A photograph of the July 10 storm taken by A. Seimon from the WP3D aircraft on the southwest side of the storm during the beginning of the supercellular stage.

extending to the ESE and the upper level divergence. Citation flight tracks in the figure show the climb just outside of the storm to gain altitude and penetrations through the anvil.

Vertical sections of the storm constructed using the CEDRIC software [*Mohr et al.*, 1986] for the same times as Figures 3 and 4 are presented in Figures 5a-5d. Note that radar cloud tops are above 14 km at all four times and at 2312 are above 16.5 km with 50 dBZ extending above 12 km. This is unusually high for storms in NE Colorado and suggests strong updrafts. The Fort Morgan sounding at 2050 and measurements from the Citation suggest the tropopause was near 12.5 km, but there is some uncertainty because 12.5 km was the maximum altitude reached by the Citation. The high radar tops can also be seen in Figure 6a, which shows the time-altitude-reflectivity profile of the storm. Different pulses of reflectivity (e.g., 50 dBZ) are apparent as different cells intensify and decay. Cell lifetime was 30 to 45 min during the multicellular stage, which is typical for storms of the high plains. Figure 6a suggests that the most intense phase of the storm occurred during the multicellular stage from 2315 to 2330. Radar tops were higher and reflectivities larger than during the later supercellular stage beginning near 0115.

3.2. Lightning Evolution and Structure

Figure 6b shows 5 min averages of CG (both negative and positive) and IC lightning flash rates. In this figure the IC flashes were determined by subtracting the CG flashes observed by the NLDN from the total flash rates determined with the interferometer. With the 23 μs sampling period of the interferometer, we observed a lot of very short duration VHF radiation sources. Figure 6b shows the IC flash rates for all IC flashes detected and also the flash rates for IC flashes >1 ms duration. The ratio of IC flashes with durations <1 ms to all of the IC flashes is shown in Figure 6c. Figure 6c also presents the ratio of all IC flashes to the total lightning (IC + CG) flash rate. Note that the ratio of IC to total lightning is >95% during much of the storm history.

In comparing the reflectivity history of Figure 6a with the lightning history of Figure 6b, it is interesting to note the association of lightning activity, particularly of IC flashes, with the cellular structure and periods of growth of the storm. This time coincidence has been observed before [e.g., *Lhermitte and Williams*, 1983]. The correlation is not strong, and, in fact, if one examines the ratio of IC flashes to total lightning (CG + IC) shown in Figure 6c), the pattern changes as different cells grow and decay. *Lang et al.* [2000] showed that much of the CG lightning during the multicellular stage occurs in the weaker cells on the NW side of the line, while the more intense cells produce mostly IC flashes. Overall, the storm produces predominantly IC lightning, particularly during the more intense multicellular phase from 2235 to 2345 and the supercellular stage. Total lightning frequencies up to 1 every 2 s (150 per 5 min) occurred during the supercellular phase. Flash rates of 1/s or more have been observed previously in convection with

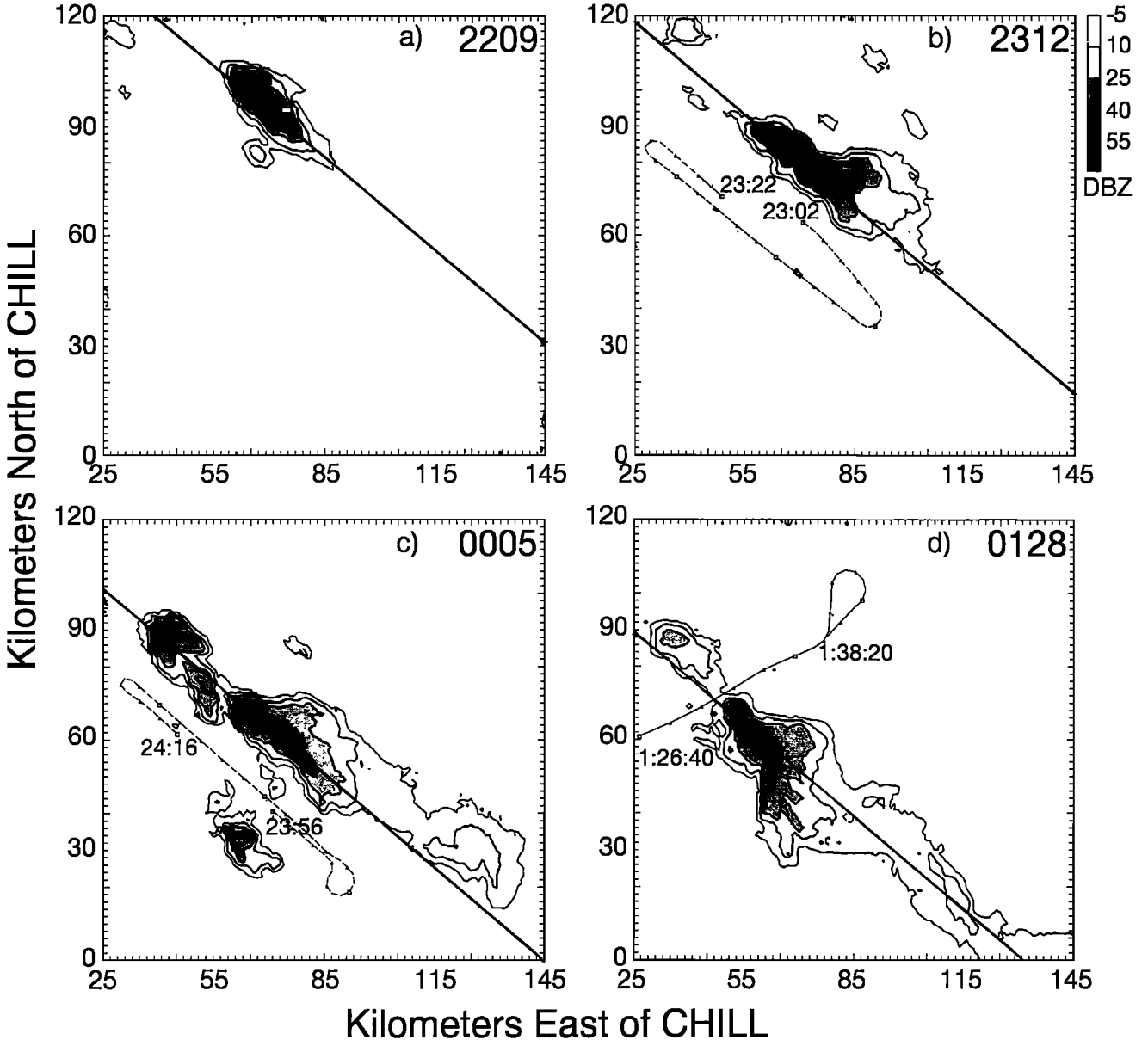

Figure 3. Horizontal sections (CAPPIs) from the CSU-CHILL radar for the July 10 storm showing the reflectivity structure at 4.5 km msl during (a) the early phase, (b and c) the multicellular phase, and (d) the supercellular stage. Tracks of the W3PD are depicted for 20 min segments centered on the time of the CAPPI. Diagonal lines indicate the locations of the vertical sections shown in Figure 5.

very strong updrafts, sometimes with little CG lightning. *Rust* [1989] found ratios of IC/CG flashes in excess of 95% in severe Oklahoma storms and thought this was probably an underestimate and pointed out that the number of IC flashes detected is dependent upon the sensitivity of the detection technique. Likewise, in the February 1998 tornadic storm in Florida, total flash rates of >1/s were observed with predominately IC flashes [*Williams et al.*, 1999] using the Lightning Detection and Ranging system at the Kennedy Space Center [*Maier et al.*, 1996].

The observation of short-duration discharges has been reported by other investigators with ground-based measurements [e.g., *Willett et al.*, 1989] and from satellite [*Holden et al.*, 1995; *Smith et al.*, 1999]. These are sometimes referred to as compact intracloud discharges. Although of very short duration (sometimes <10 μs), they are estimated to extend vertically over distances ~1 km [*Maier et al.*, 1996] with peak currents of 10 to 100 ka [*Smith et al.*, 1999]. Because of the very short duration, slow antennas and other detection techniques with only millisecond time response are not likely to detect the compact intracloud discharges. Hence they would not normally be included in many previous IC flash rates or IC/CG flash ratios. However, because of the high currents the compact discharges probably produce NO. As seen in Figure 6c for the July 10 storm, flashes ≤1 ms duration constituted from 10% to 40% of all IC flashes. The fraction would be only slightly less if we use durations of ≤10 ms.

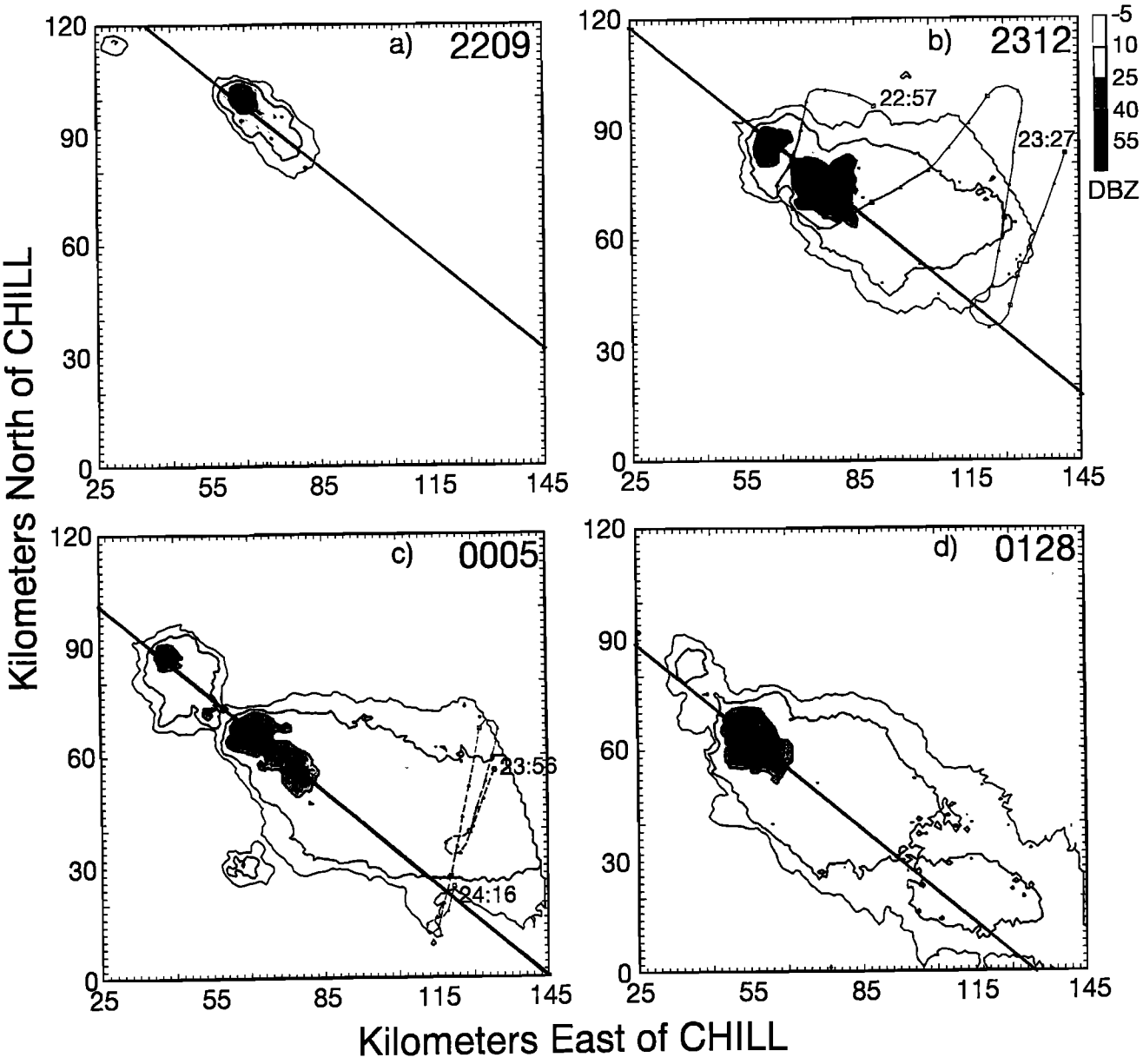

Figure 4. As in Figure 3, except CAPPIs at 10.5 km with 20 min of the UND Citation flight track superimposed. Some parts of the anvil in Figures 4b, 4c, and 4d extend beyond the maximum 150 km range of the CHILL radar.

The ratio does vary between various stages of the storm, with the highest ratios occurring during the intense multicellular stage, but with the lowest ratios during the supercell stage.

3.3. Lightning Locations in the Storm

The horizontal *x,y* locations of all individual VHF sources emitted during the 6 min time periods of the CHILL radar volume scans are superimposed in Plate 1 on the 10.5 km radar CAPPIs of Figures 4a-4d, which as discussed earlier show storm structure at different stages. The VHF sources in the northernmost cells in Plates 1a-1c, which are close to the edge of the interferometer lobes, display obvious radial dispersion, with some sources extending outside of the radar boundaries. See Appendix B for a discussion of radial dispersion and source position uncertainties. There are several interesting features seen in these overlays of VHF sources on radar contours. First, note that in these cells the sources are contained within the 10.5 km echo boundary (except when radial dispersion is a problem near lobe boundaries), but appear to extend outside of the echo boundaries at 4.5 km and 7.5 km. Although not shown, the outer reflectivity contours at 7.5 km are very similar to those at 4.5 km. This suggests to us that the lightning discharges extend up into portions of the diverging and spreading anvil. However, they remain close to the cell cores and rarely extend extensively into the downwind anvil. *Stith et al.* [1999] showed an exception for the July 10 storm where a discharge did extend some 50 to 60 km into the anvil, but this was rare for the July 10 storm.

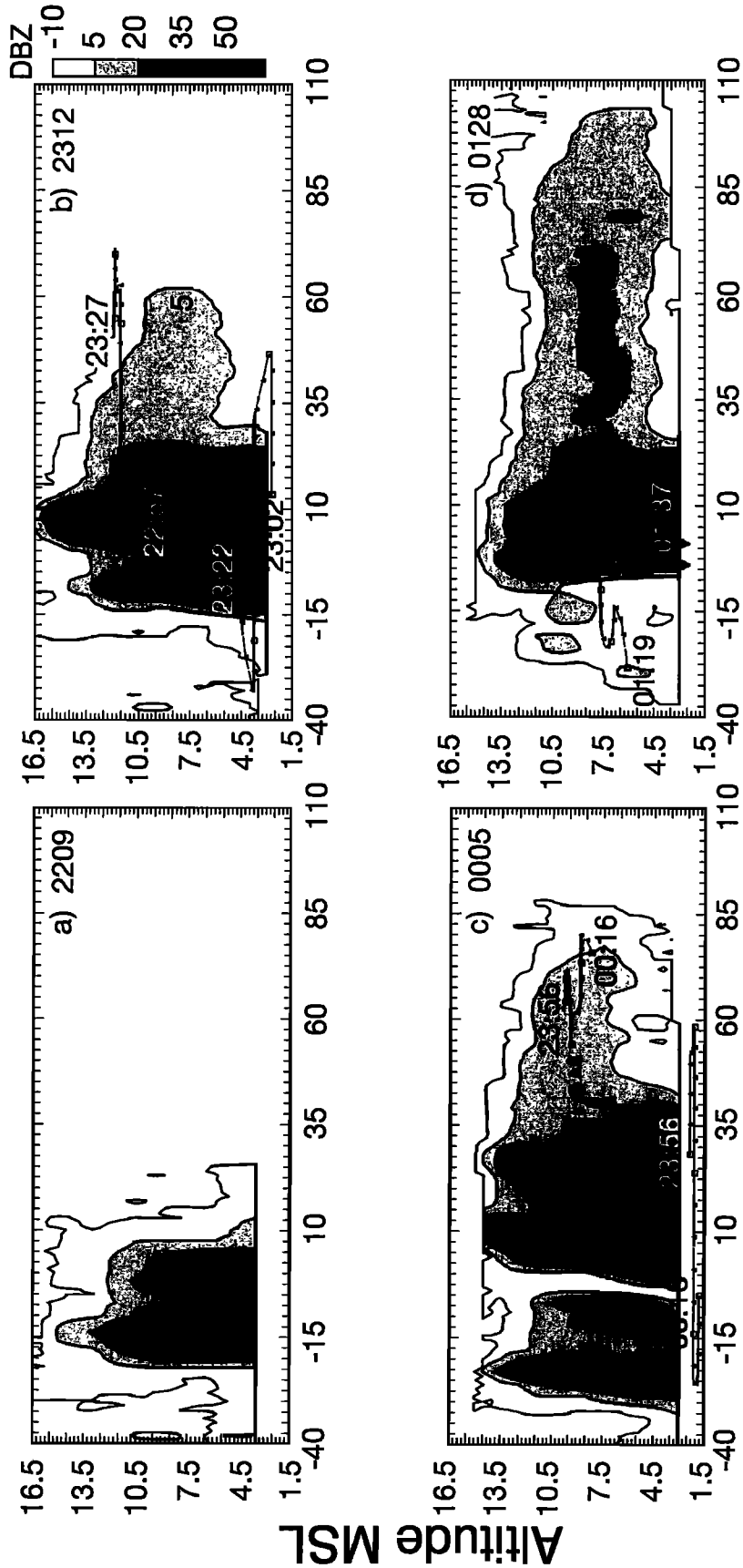

Figure 5. Constructed vertical sections through the core of the storm for the same times as those in Figures 3 and 4. The projections of Citation and WP3D tracks are superimposed. The Citation did not penetrate the core of the storm in Figure 5b, but skirted on the outer edge of the storm before penetrating the anvil at 11.6 km 10 - 15 km downwind of the core.

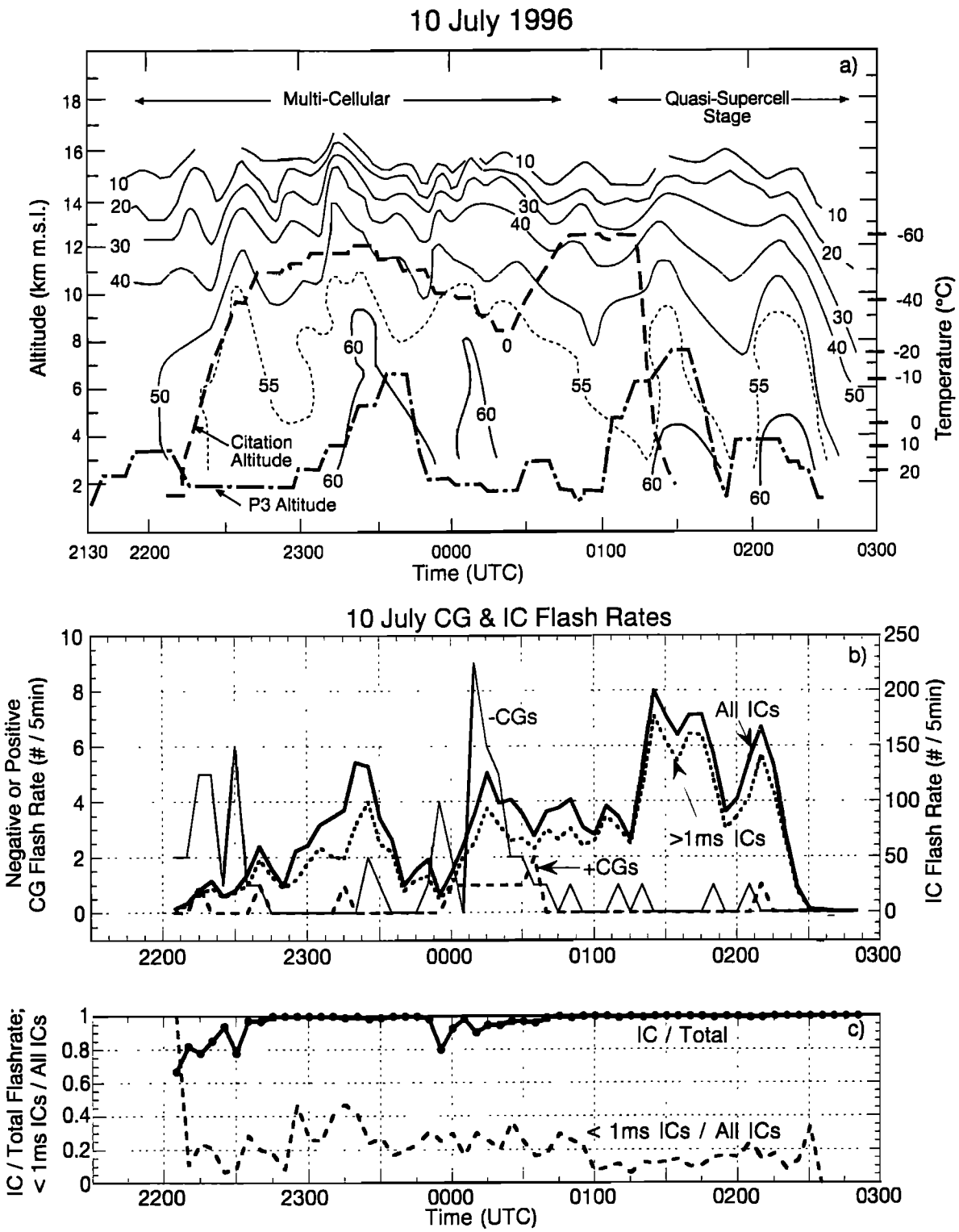

Figure 6. (a) The time-altitude-reflectivity profile of the storm, showing the evolution of the maximum reflectivity as a function of time and altitude anywhere in the storm. The flight altitudes of the Citation and WP3D aircraft are superimposed but only represent the altitude at which they were flying. (b) The IC and CG flash rate histories measured by the ONERA interferometer (total lightning) and National Lightning Detection Network (CG only). Note that the scale for IC flash rates shown on the right is 25 times that for the CG flash rate shown on the left. IC flash rates are shown for all IC flashes and also for flashes with durations >1 ms (see text). (c) The ratio of IC to total lightning during the storm evolution and the ratio of IC flashes with durations <1 ms to all IC flashes.

Also note in Plate 1c at 0005 the VHF sources in a small but newly growing region in the southeast part of the northwestern cell.

As discussed in Appendix B, the capability of the interferometer to provide reliable altitude measurements for STERAO is dependent upon range from the northern antenna site. For the early multicell phase of the July 10 storm (Figures 3a, 4a, and 5a) the cells were 50 to 60 km from Grover, but the storm gradually moved to within 25 to 40 km range during its later phases (Figures 3c, 3d, 4c, 4d, 5c, and 5d). Consequently, in the early stages of the storm, altitude information from the interferometer is limited to altitudes above 9 to 10 km and in the later phases to altitudes above ~5 to 7 km msl. Thus it is difficult to say much about the vertical distribution of lightning in STERAO storms.

In order to address the question of where NO_X from lightning might be produced and subsequently transported by storm-scale circulation, it is necessary to know the location of lightning discharges within the storm relative to storm airflow patterns. Plate 2a shows results of a Doppler retrieval for 6.9 km centered on 2313 with derived horizontal airflow vectors relative to the storm (storm motion of u,v = 1.7, -5.5 m s^{-1} was subtracted). Horizontal winds were derived from the Doppler radar velocities by an overdetermined two-component regression. Vertical air velocities (w) were deduced by the vertical integration of the mass continuity equation. The vertical velocities in a column were taken to be a linear combination of (1) the vertical velocity deduced from a downward integration from a boundary condition (w = 0) at the top of the echo and (2) the vertical velocity produced by solving an overdetermined variational problem (similar to *O'Brien* [1970]) with upper and lower boundary conditions (both w = 0). The coefficients of the linear combination are related to the distance between the lowest horizontal divergence in a column and the Earth's surface and reflect the fact that the variational formulation is fully appropriate only when the measurements of horizontal divergence extend to the Earth's surface. As with all Doppler retrievals of vertical velocity it is difficult to give a good estimate of errors, especially since it is likely that the errors are correlated [*Matejka and Bartels*, 1998]. We expect errors in vertical velocity of 1 m s^{-1} to a few meters per second and probably more for small-scale (<2 km) features.

An interesting finding emerges when the VHF lightning sources from 2310 – 2315 are overlaid on the updraft – downdraft structure and airflow pattern obtained from the Doppler radar retrieval centered on 2313 Plate 2b. The storm was in a very active stage of development at this time with the Doppler-derived vertical motions showing a main updraft core located near x,y = (72,73) with speeds of 18 m s^{-1} extending from 8.5 to 11 km and 16 m s^{-1} at 6.9 km. A surprisingly strong downdraft near x,y = (71,78) starts at 9.5 km with speeds of 8 m s^{-1} at 6.9 km and –15 m s^{-1} near cloud base. This downdraft appears to have been forced by precipitation loading. The Doppler analysis used a 2 km filter, so small-scale updrafts and downdrafts might be larger. A 3-D simulation of the storm [*Skamarock et al.* 2000] produced maximum updrafts of 25 –30 m s^{-1}.

Note in Plate 2b that very few sources were detected in the region of the main downdraft. Some sources were located in the active updraft core, but not many. The majority of the sources are located in the moderate updrafts and downdrafts, and downshear of the main updraft/downdraft couplet, with a tendency to be located in the downshear portion of higher reflectivities. Even for the weaker northwestern cell the VHF sources from lightning tend to be in regions of updraft, with only a few sources in the weak downdraft. If found to be true at other times and for other storms, this finding may have important implications for the vertical redistribution of NO_X resulting from lightning.

Because of the difficulty of obtaining spatial and temporal coverage of both lightning and air motions inside storms, there are relatively few publications relating the location of lightning to vertical air motion structure. Of work that has been published [e.g., *Lhermitte and Krehbiel*, 1979; *Lhermitte and Williams*, 1983; *Ray et al.*, 1987], there is not a consistent picture of where lightning occurs relative to updraft/downdraft structure, but there are insufficient observations to examine this in a 3-D time-evolving context. The excellent work of *Proctor* [1991] in this and his other publications shows that lightning most often begins in the upper region of high reflectivity near 20 dBZ and then moves to weaker reflectivity, but he had no direct measurements of vertical air motion other than inferred from reflectivity measurements. More work is needed to better understanding these relationships.

3.4. Measurements of Tracers

To determine the impact of deep convection on the chemical composition of the troposphere by transport or by lightning production of NO_X (=NO + NO_2), it is essential to know the mixing ratios of constituents both in the air flowing into the storm from the boundary layer and in the air exiting in the anvil. It is also important to know the concentrations at middle and high altitudes outside of the storm because turbulent mixing of environmental air into the storm updrafts can affect the concentration of chemical species in the storm. During STERAO we found both horizontal and vertical gradients of constituents in the environment, particularly in the boundary layer. For the July 10 case, ozone and carbon monoxide (CO) were used as tracers to examine the mass of air transported from below.

Combined vertical profiles of CO and ozone from the Citation outside of the anvil, and from the WP3D (which was only very briefly in cloud near cloud base) are shown in Figure 7a. The Citation measurements in the anvil are shown in Figure 7b. Only observations from within 50 km of the storm are included for the WP3D in this figure. All Citation measurements except those very close to the airport (those below 1.8 km) were included because these are the only lower-altitude measurements from this platform. The ozone profiles in the boundary layer show relatively little variation, with values of 60 ± 10 ppbv (parts per billion by volume). The CO values in roughly the lowest kilometer are 135 ± 10 ppbv decreasing to 120 ± 10 ppbv at 4 km (also see Plate 3). Both constituents have minima in the midtroposphere from 6 to 8 km. Above 8 km the ozone profile increases to >300 ppbv as the Citation approaches the tropopause and exhibits lots of variability, evidence of horizontal and vertical inhomogeneity. The values of ozone are generally smaller in the anvil than

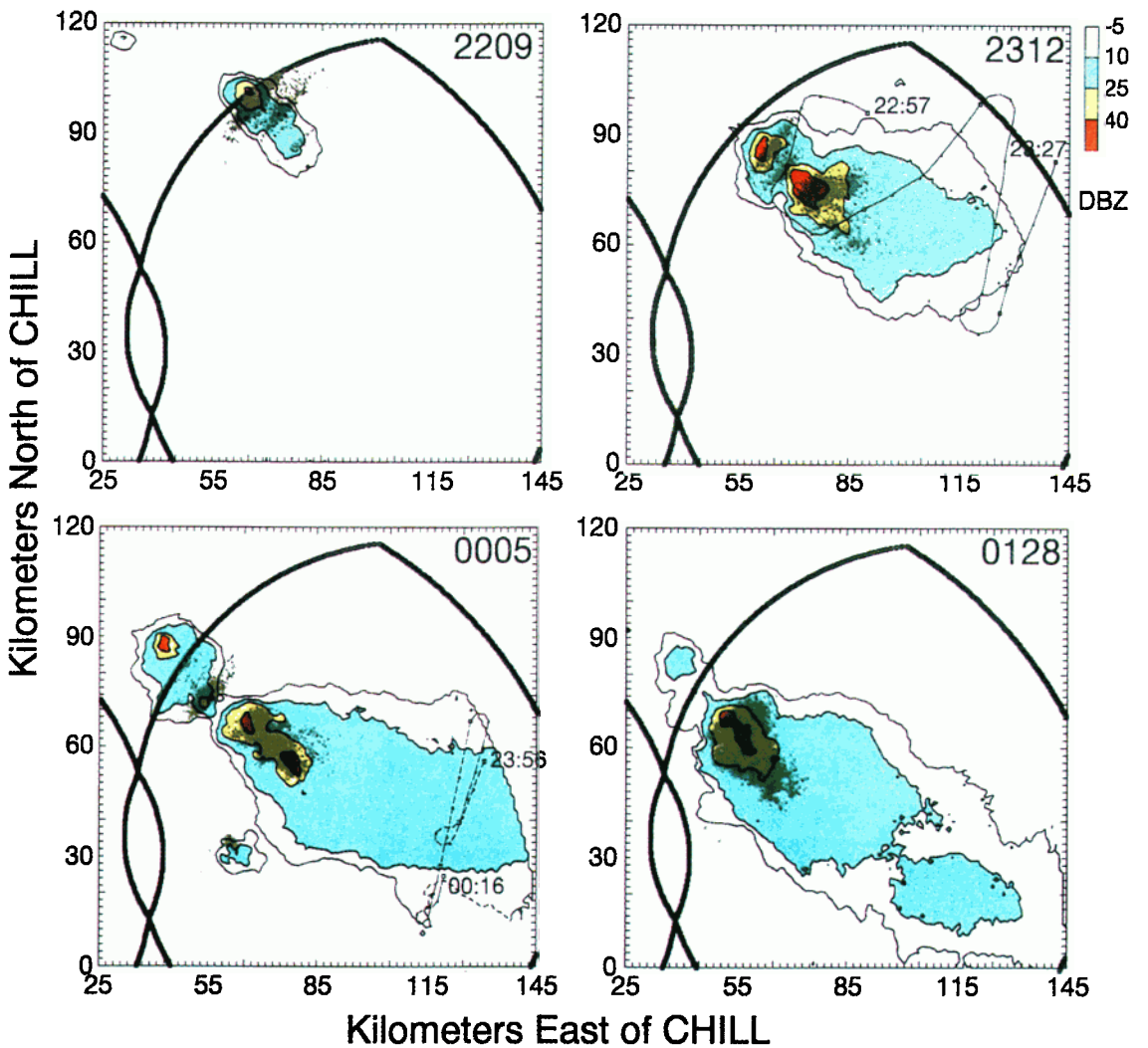

Plate 1. All VHF sources from lightning detected by the ONERA interferometer during the 6 min period taken to complete the separate radar volume scans for Figures 3, 4, and 5 superimposed on the radar CAPPIs for 10.5 km msl. Part of the northwestern cell in Plate 1c is outside of the interferometer lobe.

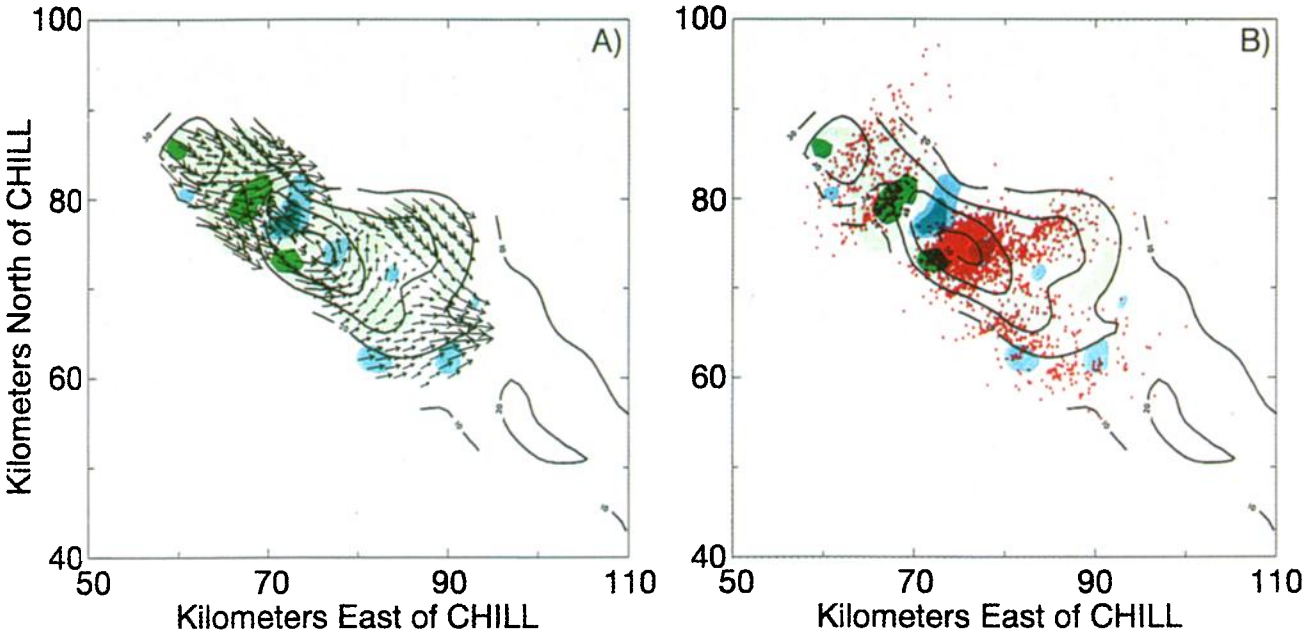

Plate 2. (a) Doppler radar retrievals centered on 2313 UTC of horizontal air motion (shown by vectors with lengths corresponding to the distance moved in 300 s) and vertical motion, with updrafts from 0 to 8 m s^{-1} shown in light green shading, updrafts >8 m s^{-1} in dark green shading, downdrafts <-2 m s^{-1} in light blue, and downdrafts < -8 m s^{-1} in dark blue. Contours of reflectivity are superimposed beginning at 10 dBZ and increase in increments of 10dBZ. (b) Same as Plate 2a, except with wind vectors replaced by VHF lightning sources in pink for the period 2310 to 2315 UTC. The curved, bold line in the upper left corner of Plate 2b shows the interferometer lobe boundary.

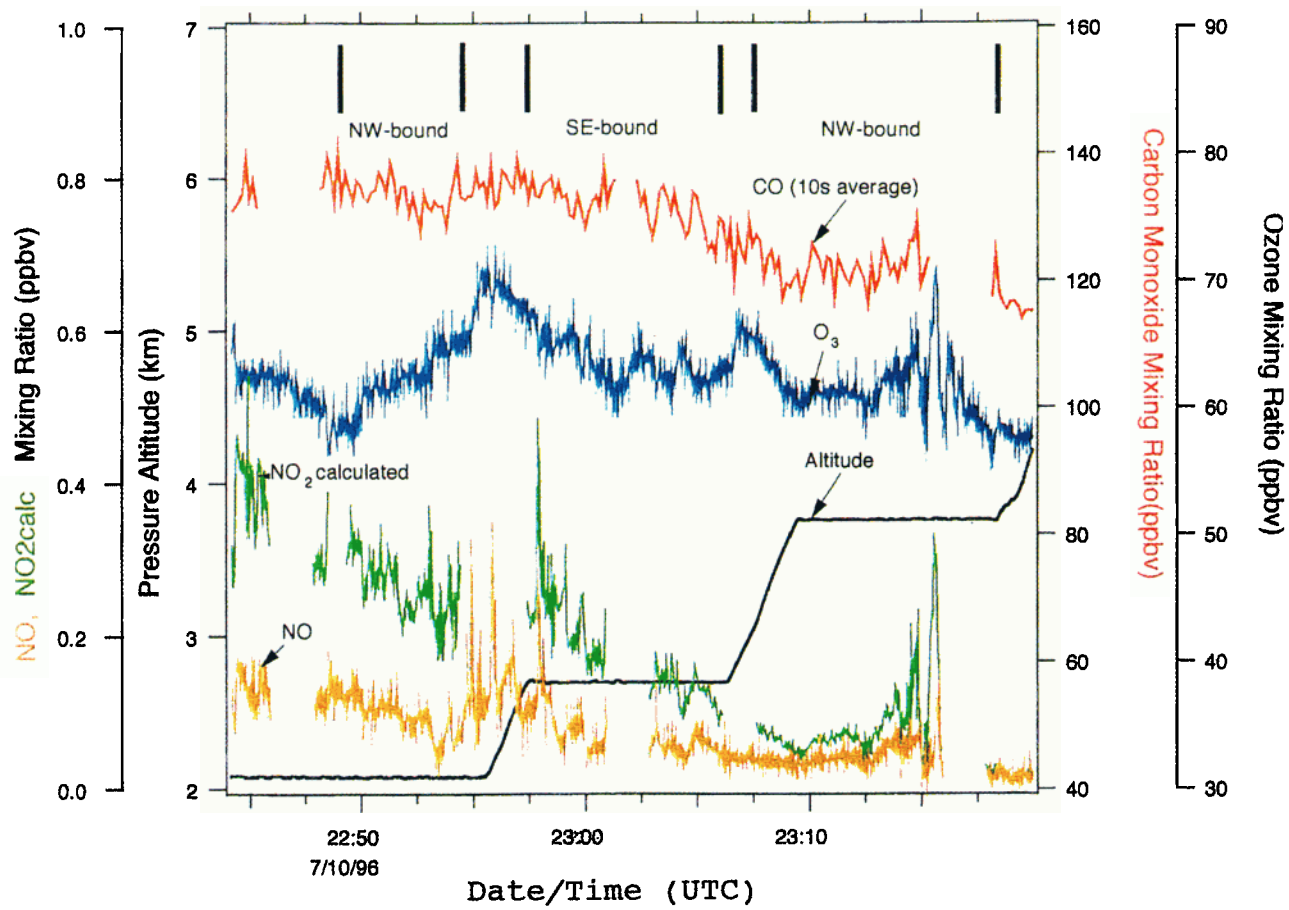

Plate 3. Measurements of NO, NO_2, ozone, CO and altitude made by the WP3D aircraft in the boundary layer from 2245 to 2320 UTC during the early phase of the storm.

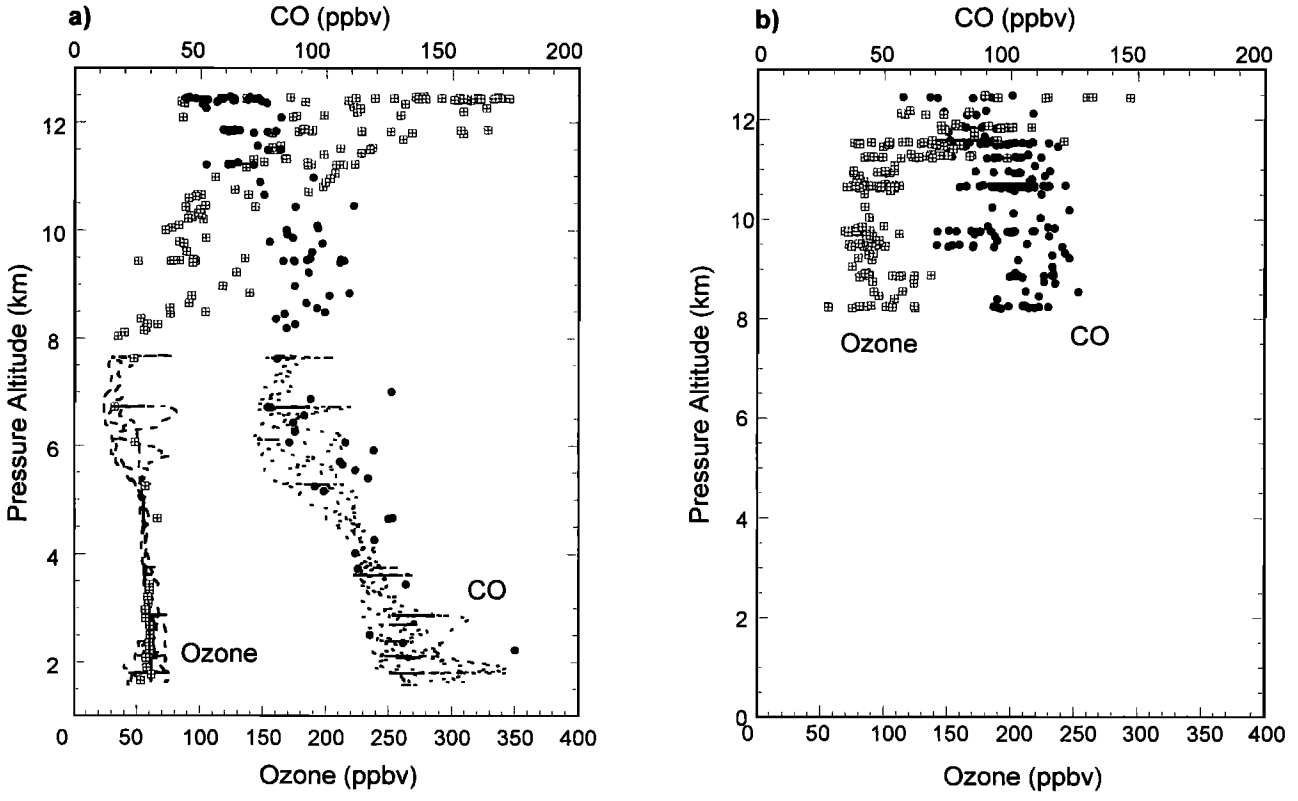

Figure 7. Vertical profiles of ozone and CO from the WP3D (10 s averages) and from the Citation (30 s averages). (a) Only out-of-cloud measurements for altitudes >1.8 km msl are shown for the Citation, and WP3D measurements are limited to within 50 km of the storm. (b) Citation measurements inside the anvil are shown.

outside, although some larger values are also seen at the edge and top of the anvil. Outside of the anvil, CO gradually decreases from 100 ± 10 at 9 km to 60 ± 15 ppbv at 12 km. Inside the anvil the larger CO values were 100 to 120 ppbv, almost as large as those seen in the upper boundary layer, suggesting relatively little entrainment of environmental air into some parts of the anvil. At the upper levels outside of the cloud, CO is anticorrelated with ozone, which is typical for the upper troposphere and lower stratosphere.

3.5. Measurements of Nitrogen Oxide in the Environment and in the Anvil

Altitude profiles of NO from both the WP3D and the Citation are depicted in Figure 8. Because NO_X = NO + NO_2 would be essentially conserved (but not NO or NO_2) over the short timescale required for vertical transport from the boundary layer to the anvil region, an estimate of NO_{XC} = NO + NO_{2C} for the lower altitudes covered by the P3 is included. NO_{2C} is a calculated estimate of NO_2. This estimate is based on the photochemical steady state relationship $NO_{2C}/NO = k_{NO/O3}[O_3]/J_{NO2}$, where $k_{NO/O3}$ is the rate coefficient for the NO + O_3 reaction at the temperature of the constituent measurements and J_{NO2} is the photolytic conversion rate for NO_2 to NO. Radiometric measurements made on the WP3D [*Frost et al.*, 1998] were used to derive J_{NO2}. It is more difficult to estimate NO_X from the NO measurements inside the anvil. At the higher altitudes inside the anvil, the NO_2/NO ratio is expected to decrease substantially from that for the lower troposphere so that NO should more closely approximate NO_X. However, radiometric or actinic flux measurements were not made on the Citation, and because of the complications of calculating J_{NO2} within the cloud, no precise estimate of NO_{XC} can be made for all altitudes within the anvil. In the bright upper part of the anvil, photolysis frequencies are likely to be larger than clear sky values [*Madronich*, 1987] so that the NO_2/NO ratio of 0.3 calculated for clear sky conditions is likely valid to within a factor of 2. In these circumstances the NO_X/NO ratio would be in the range of 1.1 to 1.6. In the more optically thick lower part of the anvil, larger NO_2/NO ratios would be expected, but insufficient information is available to make a reasonable estimate of J_{NO2}. For comparison, however, *Huntrieser et al.* [1998] reported measured NO_X/NO ratios of 1.3 – 1.8 at altitudes of 8, 9, and 10 km in late afternoon storm anvils over Germany, but they did not report at what altitudes with respect to anvil thickness the penetrations were made.

From Figure 8 we see that the maximum values of NO in the anvil are comparable to NO_{XC} in some locations in the lower boundary layer during the WP3D flight. If taken at face value without further analysis, this suggests that transport from the boundary layer might have been the primary contributor of the NO_X observed in the anvil and that the contribution from lightning was small. However, note the large variation in NO and NO_{2C} values at altitudes below 4 km from the WP3D in Plate 3. (The legs at 2.7 and 3.8 km in Plate 3 are the two legs shown in Figure 3b.) The largest values of NO and NO_{2C} are highly structured and

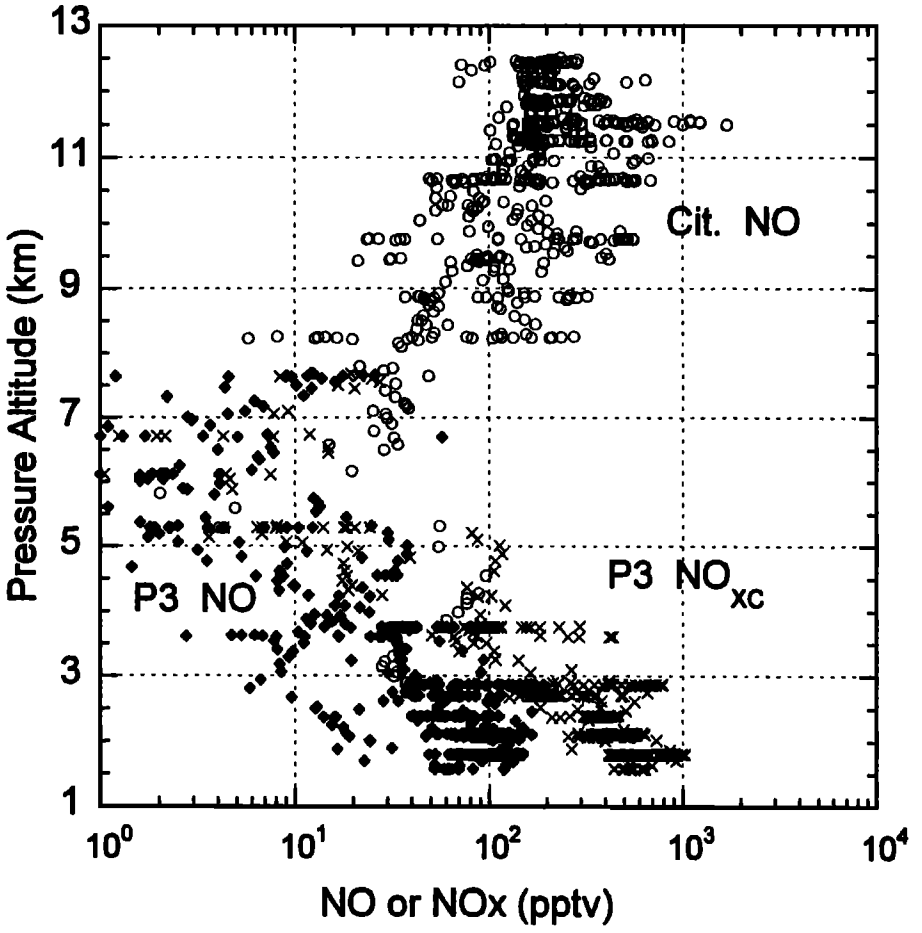

Figure 8. Vertical profile of NO measurements (20 s averages) from the Citation (2233 to 0125 UTC) and the WP3D (2245 to 0205 UTC) and NO_{XC} (NO + NO_{2C}) calculated values from the WP3D. Only measurements made in the vicinity of the storm are included for the WP3D.

were found on the western side of the storm downwind of Greeley and the Denver metropolitan area. The plate shows that in addition to large horizontal variations there were appreciable vertical gradients in the boundary layer, with smaller values at higher altitude. The wind directions along the track at 2.1 km were from about 160° to 190° as the WP3D moved from southeast to northwest, while at 2.7 km they were from 210° in the east and 270° in the west. For the 3.8 km pass they were northwesterly from 320° to 340° in both the east and west. Thus the environmental winds exhibited significant directional shear.

The paper by [*Skamarock et al.* 2000] presents results from a cloud-resolving model simulation of the storm and discusses environmental winds and airflow into the storm in more detail. The cloud simulation suggests that it is not likely that the storm ingested air from lower than 500 m agl (≈2 km msl), especially in its early phase. The air in the lowest levels of the boundary layer probably was not lifted sufficiently to enter the storm. The simulation suggests that the main source of air feeding the storm was from the middle to upper part of the boundary layer. If this is correct, an examination of Plate 3 suggests that mixing ratios of NO_X ingested by the storm would have been for the most part from 200 to 500 pptv, excluding a couple of small regions with larger values to 700 pptv. If the storm was ingesting air from the lowest boundary layer, NO_X values of ≈0.7 ppbv are still upper limits. The above discussion makes it clear that it is difficult to pinpoint one region of the storm as the region of inflow and the chemical composition of that inflow.

Measurements of NO, ozone, and CO made by the Citation in a series of penetrations through the anvil 50 to 60 km downwind of the active convection (see Figure 4c) are shown in Figure 9. The differences seen in the different passes reflect temporal as well as spatial variations as different cells grow and mature (Figure 6). The passes span times from 2312 to 0022 UTC and altitudes from 11.8 to 8.3 km, that is from near the top to the bottom of the anvil. With wind speeds in the anvil of 20 to 25 m s^{-1} these passes would have sampled the air exhausted into the anvil from approximately 2230 to 2330, including the period of intense convection from 2300 to 2330. During this period the vast majority of the lightning was IC (Figures 6b and 6c). Air trajectories released throughout the boundary layer in the cloud model simulation of the storm suggest that the time for transport from the boundary layer, through the storm core, and 50 km downwind into the anvil, where the anvil penetrations were made, would take a little less than one

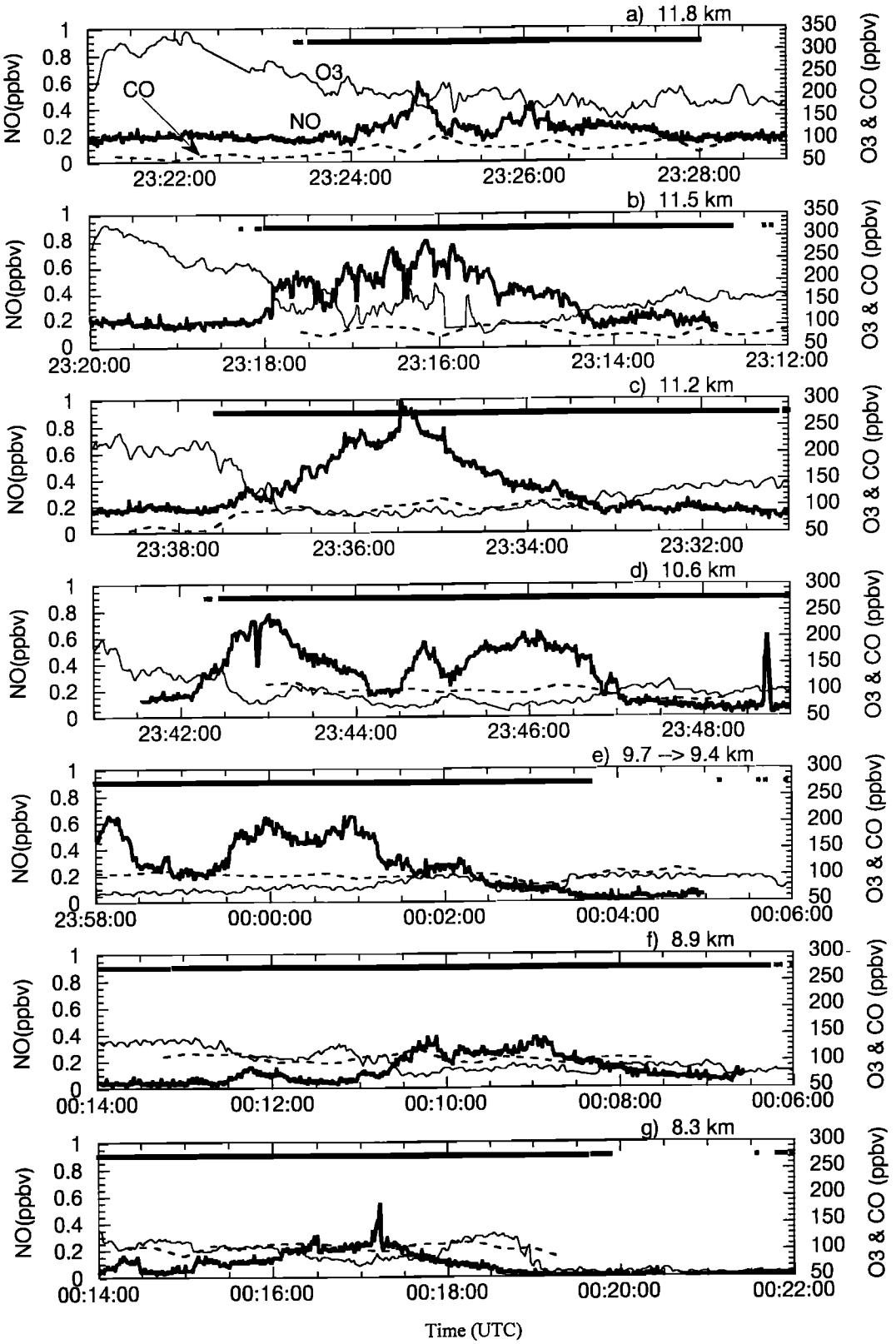

Figure 9. Eight minute segments of NO, ozone, and CO measurements made by the Citation aircraft at altitudes from 11.8 to 8.3 km msl in the anvil 50 - 60 km downwind of the storm core. The times of some passes are reversed and the order of the passes changed to display the results as if the reader is looking to the northwest into the anvil toward the storm core and viewing a cross section of the anvil. The solid, continuous line toward the top of each panel indicates times when the Citation was in cloud.

hour [*Skamarock et al.* 2000]. Thus the WP3D passes made near the storm in the boundary layer from 2250 to 2315 should have sampled air which was later observed by the Citation during the anvil passes of Figure 9.

In Figure 9 the maximum NO concentration is 1 ppbv at 11.2 km, with values of 0.8 ppbv at 10.6 and 11. 5 km. The larger NO concentrations were found in the upper half (but not very top) of the anvil. The storm remained electrically active throughout and after the period of Citation anvil penetrations, so the falloff at lower altitudes is not likely to be the result of reduced electrical activity. A later spiral ascent from 8.5 to 12.5 km in the anvil ≈75 km downwind of the core from 0024 to 0050 showed a similar NO profile as those depicted in Figure 9. This pattern of increasing NO in upper parts of the anvil was observed in other STERAO storms and also seen by *Ridley et al.* [1996] in New Mexican storms. Although NO_X partitioning will favor an increasing contribution from NO_2 in the lower and thicker parts of the anvil, Ridley et al. observed a decreasing contribution from NO_2 in the lower parts of a New Mexico thunderstorm anvil. At least for that case the contribution of NO_2 to the total NO_X in the lower anvil was not dominant. Outside of the anvil, NO values are 100 to 200 pptv at altitudes above 10 km and 50 pptv or less below 10 km. There is considerable horizontal structure within the anvil. For example, the pass at 10.6 km (Figure 9d) shows two areas of enhanced NO, probably resulting from two separate cells with both lightning and transport contributions possible. This is also seen at times in the cloud simulation [*Skamarock et al.* 2000]. The measurements in Figure 9e do not show a complete penetration of the anvil. The Citation flew about two thirds of the way through the anvil in the southerly direction (not shown), and then reversed course and flew north again. Figure 9e shows data from this northerly track.

3.6. Stratospheric Air in the Upper Troposphere

Note in Figures 9a-d that on the south side of the storm (left side of the figure) the large values of ozone are suggestive of stratospheric origin, especially the large values of > 200 ppbv at 11.2 km and above. Some evidence of enhanced values (values >100 ppbv) can be seen as low as 10.6 km, roughly 2 km below the apparent tropopause. Although ozone values on the north side of the storm exceed 100 ppbv, which is often thought of as a threshold for stratospheric air, the values on the south side are considerably larger. The measurements shown in Figure 9 were taken 50 – 60 km downwind of the core, but measurements from pass 2 shown in Figure 10 were only 10 – 15 km from the core and also show the same pattern of high ozone on the south side of the storm. Potential temperature measurements (not shown) are well correlated with ozone outside of the storm, with larger potential temperatures on the south side, which is also consistent with downward transport of stratospheric air. As commented earlier and seen in Figures 5 and 6, radar tops frequently extended to 14 km and near 2315 extended to 16.5 km. This is approximately 4 km above what we believe was the tropopause at 12.5 km, the highest altitude flown by the Citation. However, without measurements above the tropopause and horizontally away from the storm in the north-south directions, it is not possible to know if

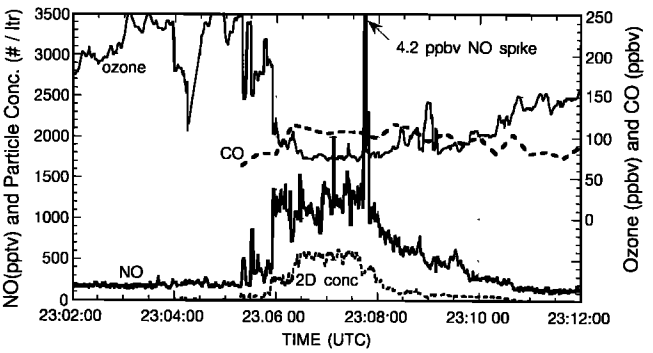

Figure 10. NO, ozone, CO, and ice particle (2D) concentrations measured by the Citation at 11.6 km msl during its second penetration through the storm from 2305 to 2311 UTC, approximately 10 - 15 km downwind of the core as shown in Figure 4b. The CO instrument was in calibration mode from 2302:30 to 2304:50, the period with the highest ozone values. For the 3 min prior to calibration the values were nominally 70 +/- 10 ppbv.

the high ozone values are a result of the effects of overshooting tops or a local discontinuity of the tropopause. It is interesting to note that the 3-D cloud simulation of [*Skamarock et al.* 2000], which used a high-resolution 1 km grid, did not reproduce this asymmetry. Although a few studies, [e.g., *Poulida et al.*, 1996] have looked at the impact of overshooting tops on stratospheric – tropospheric exchange, it remains an important topic for further study.

3.7. Transport, Mixing, and NO_X Production by Lightning

If air is lifted adiabatically without mixing from below cloud base into the anvil, values of ozone and CO in the anvil should be comparable to those feeding the storm below base. We argued earlier based on the simulations that the air encountered by the WP3D on its legs at 2.7 and 3.8 km is most likely to have been the air ingested by the storm. If the air was lifted without mixing, ozone would be expected to be 65 +/- 5 ppbv, CO values would be 120 - 135 ppbv, and the most likely values for NO_X would be 0.2 to 0.5, with a point maximum of 0.7 ppbv. These values are based on the measurements of the 2.7 and 3.8 km legs of the WP3D in Plate 3. Figure 10 presents Citation measurements of NO, CO, ozone, and ice particles made during penetration 2 through the anvil at 11.5 km. This pass was only 10 to 15 km downwind of the reflectivity core (the SW to NE pass in Figure 4b) and before appreciable mixing in the anvil is likely. The Citation was nearest the highest reflectivities, updraft core, and divergent outflow into the anvil (Figure 4) from about 2305 to 2308.

Flat, horizontal concentration profiles in growing cumulus clouds often suggest the possibility of nearly unmixed ascent of the air from below cloud base. As air ascends in the updraft, there is entrainment and erosion of the core updraft on the periphery, but the core can remain unmixed and maintain a flat profile. For the 2306 to 2308 period (Figure 10), the ozone trace is relatively uniform with values of 75 +/- 5 ppbv. Recall from section 2.5 that the intercomparison flights showed Citation ozone values to be greater than those of the WP3D with a 5 ppbv offset.

Accounting for this difference yields ozone values of about 70 ppbv across this flat profile, only slightly greater than the WP3D boundary layer values of 65 +/- 10 ppbv and within the instrument uncertainties listed in Tables 4 and 5. Furthermore, the CO trace is also relatively flat, varying from 100 to 115 ppbv, which is slightly less than the boundary layer values. However, the 20 s averaging necessary with the Citation CO measurements, the correction factor of 1.20 applied for this day, and the general noisiness of the CO signal on the Citation make these measurements less reliable than ozone. The flat profiles of ozone and CO from roughly 2306 to 2308 with values that are very near those measured in what we believe was the inflow of the storm strongly suggest that the air encountered by the Citation during this period was relatively unmixed. We can not quantitatively determine the degree of mixing, because the accuracy of the measurements is insufficient, because both ozone and CO have low values in the midtroposphere with little gradient, and because we have no measurements in the core of the storm. The slightly greater ozone values observed during pass 2 could have been the result of mixing of environmental, low-ozone midtropospheric air, followed by mixing of ozone-rich air at higher altitudes. However, the fact that CO is only slightly lower in the anvil than in the middle to upper boundary layer, in spite of CO being appreciably lower in the middle and upper troposphere, is consistent with little mixing of environmental air into the updraft core and in the anvil closely adjacent to the core.

Turning now to the NO measurements shown in Figure 10, we see that the NO values from 2306 to 2308 (corresponding to roughly a 12 km path length) are choppy but relatively uniform, with values from 1 to 1.4 ppbv, except for the sharp spike of 4.2 ppbv at ~2307:45. This spike of NO is likely to have originated from nearby lightning slightly before the Citation penetration. See the paper by *Stith et al.* [1999] for additional details. The values of 1 to 1.4 are much larger than the estimated values of NO_X in the middle to upper boundary layer of 0.2 to 0.7 ppbv from the WP3D measurements. As discussed below, lightning has made a significant contribution. The flat nature of the NO profile suggests that the distribution of lightning-produced NO_X in the region feeding the anvil of the storm was relatively uniform and/or that turbulent mixing within the updraft was effective at smearing out the individual sources of NO originating from lightning.

The evidence above suggests that the air in the region with a flat ozone profile in pass 2 was lifted from the boundary layer to this location relatively unmixed. Thus NO_X expected by transport alone would be roughly from 0.2 to 0.5 ppbv, with a maximum of 0.7. The average concentration of NO from the Citation between 2306 and 2308 is approximately 1.2 ppbv, excluding the large spike of 4.2 ppbv near 2307:45. An observer on the Citation noted that it was bright inside the anvil and concluded the pass was relatively near the top of the anvil. This being the case, a reasonable range for the NO_X/NO ratio would be 1.1 to 1.6, as discussed previously in section 3.5. Assuming a NO_X/NO ratio of 1.1 to 1.6 gives values of NO_X of 1.3 to 1.9 in this region. Hence, using this scenario for the 2306 to 2308 period, lightning contributed 60-90% of the estimated NO_X mixing ratios. Conversely, transport accounted for 10-30%. A minimum contribution of 45% from lightning is obtained for the maximum NO_{XC} value of 0.7 ppbv observed in a small region during the WP3D leg at 2.7 km. It is not possible to refine this estimate without measurements in the anvil of NO_2 or of actinic flux and a more uniform distribution of NO_X entering the storm at cloud base.

It is important to note that the air observed during pass 2 probably originated at cloud base as little as 15 to 20 min earlier and would have been passing through the 6 to 8 km altitudes 10 to 15 min earlier. The -10° to -20°C (6 to 8 km for this case) region of thunderstorms is frequently the altitude at which lightning (both IC and CG) originates [*Krehbiel*, 1986; *Proctor*, 1991]. Figure 6 shows that only IC lightning occurred 20 min prior to 2305 and only three CG flashes for the 30 min period prior to 2305. This should be compared to the over 300 IC flashes for this same 30 min period. There is little doubt that the vast majority of NO_X produced by lightning in this storm was from intracloud lightning.

4. Concluding Remarks

The STERAO Deep Convection experiment provided a wealth of chemical, lightning, and kinematic measurements with which to examine the transport of constituents from the lower to the upper troposphere, the production of NO_X by lightning, and lightning characteristics in relationship to storm structure for storms of NE Colorado. As an example we have presented observations of storm structure and lightning evolution over the entire 5 hour history of the July 10 storm, that is from before the first lightning flash to the decay of the storm. Additionally, the WP3D observations acquired before thunderstorm development gave information on the distribution of constituents for a convective regime. Interferometer measurements in combination with the National Lightning Detection Network allowed us to determine the flash rate history for both IC and CG lightning for a range of storm types over a several hundred square kilometer region extending from the foothills of the Rocky Mountains to the plains of NE Colorado. The measurements show the value of detecting not only CG lightning, but also IC flashes, particularly for more intense convection where IC flashes can dominate. As in the case discussed here, the scenario emerging from recent research is that an abrupt increase in IC flashes is often a good indicator of the onset of intense updrafts in a storm. Further work is needed, but knowledge of both IC and CG flash rates in real time might potentially aid in the nowcasting of incipient intense convection producing tornadoes, hail, or severe winds. The outbreaks of tornadoes in Florida in February 1998 were preceded by abrupt increases in IC and hence total lightning *[Williams et al.*, 1999]. The difficulty of obtaining intracloud or total flash observations, especially over a large area, suggests the importance of geostationary satellite observations.

As has been shown by a number of other investigators [e.g., *Dickerson* et al., 1987, *Smyth et al.*, 1996, *Pickering et al.*, 1998], thunderstorms can be very effective in transporting species from the boundary layer to the upper troposphere. For the July 10 case we have shown that the storm lifted boundary layer air with relatively little mixing

into the anvil close to the storm core. As the air moves further into the anvil additional mixing occurred. [*Skamarock et al.* 2000] further examine the mixing using both the observations and a 3-D cloud-resolving model simulation of the storm.

In this and other STERAO storms the highest values of NO were found in the middle to upper half of the anvil. This is consistent with the study by *Ridley et al.* [1996] for storms in New Mexico in a region with little anthropogenic influence. In northeast Colorado, where anthropogenically produced NO_X sources exist, it is first necessary to quantify transport and mixing of anthropogenic sources of NO_X before assessing the production of NO_X by lightning. Using a simple approach we have estimated that for one period of the storm's history the most likely contribution of NO_X due to lightning is 60-90%, with a minimum of 45%. It is difficult to refine this contribution because of the inhomogeneous distribution of NO_X in the boundary layer, the difficulty in identifying the dominant region of inflow in the storm, the lack of NO_2 measurements in the anvil, and insufficient measurement accuracy of the tracers.

For the July 10 case it is clear that the NO_X produced by lightning was almost exclusively from IC lightning. During the half hour period 2235 to 2305, immediately prior to intensive Citation observations in the anvil, there were only three CG flashes compared to more than 300 IC flashes. Yet the values of NO (and estimated NO_X) observed in this storm are within a factor of 2 of the values of NO (NO_X) observed in other STERAO storms and in New Mexican storms studied by *Ridley et al.* [1996] and the estimated lightning-produced NO_X found by *Huntrieser et al.* [1998] in anvils in Germany. These observations suggest that IC lightning may be a major source of NO_X contrary to what is commonly thought. For the 2235 to 2305 period the IC/CG ratio was ~100/1. For the supercellar period from 0100 to 0200 there were only three CG flashes but over 1600 IC flashes (with more than 1400 having durations >1 ms), giving an IC/CG ratio of ~500/1. For the storm as a whole the IC/CG ratio was >100/1. These values are far different than frequently quoted numbers of between 3/1 and 10/1 [e.g., *Price et al.*, 1997]. New techniques are showing that in severe supercell storms lightning can be essentially continuous [*Krehbiel et al.*, 1998]. In these circumstances use of flash rates to determine impact on NO_X production becomes questionable. In many meteorological phenomena it is often a small fraction of the total events that contribute most to the overall impact of the phenomena. It would not be surprising if this is also true of NO_X production by lightning. The most intense storms with copious IC lightning such as storms in the Great Plains of the United States [*Krehbiel et al.*, 1998] and in the tropics [e.g., *Rutledge et al.*, 1992] may be the major contributors to regional and global budgets. This is contrary to the studies of *Price et al.* [1997] and others, where the assumption is made that NO_X production by individual IC flashes is 10 times less than for CG flashes. Thus they conclude that even though there are more IC flashes than CG, the overall contribution of IC lightning is less. Most segments of lightning, including both negative and positive leaders as well as return strokes and recoil leaders, produce ionized channels, which require temperatures in excess of 5000 K (M. Uman, V. Rakov, and A. Bondiou-Clergerie, personal communications, 1999). Because it is generally believed that temperatures of 2500 to 3000 K are sufficient to "freeze out" NO [*Chameides*, 1986], it seems likely that most discharge processes of both IC and CG lightning can produce NO in appreciable quantities. For example, *Orville* [1968] estimated a temperature of 30,000K for a leader step and 20,000K for dart leaders [*Orville*, 1975]. Negative leaders in clouds have similar behavior to stepped leaders, and recoil streamers have similar behavior to dart leaders.

Although we have not addressed the problem herein, the STERAO observations did not reveal large enhancements of NO_X in the outflow below cloud base. We attempted to investigate the outflow region on several occasions, but it is difficult to accomplish because it requires identifying the region of outflow in real time and flying the aircraft at low levels in regions with moderate to large reflectivities and possible hail and turbulence. Nonetheless, on those occasions when low-level passes in outflow regions were made, large enhancements were not found. For the July 12 storm, M. Trainer concluded that an enhancement of ≈200 pptv of NO_X below cloud base probably occurred. This is much smaller than the typical enhancements of 1 to 2 ppbv seen in upper anvil regions by *Ridley et al.* [1996] in New Mexico, *Huntrieser et al.* [1998] in Germany, and in STERAO. It is puzzling why larger enhancements are not found below base, particularly in view of the pioneering work of *Noxon* [1976] and other ground-based measurements. Are we not flying in the right region at the right time? This mystery deserves additional study. One possible explanation does emerge from the superposition of combined Doppler radar air motion retrievals and the VHF lightning sources in Plate 2, which shows relatively few VHF sources in the region of the downdraft core. The vast majority of the lightning channels appear to be in moderate updrafts and not in the strong downdrafts. This result pertains to only one 5 min period for this one storm. It clearly needs additional study, but is an intriguing finding.

In this paper and the paper by [*Skamarock et al.* 2000] we have presented observational and simulation results from only one storm, but as seen in Table 1 many storms were observed which are deserving of further study. *Lang et al.* [1999] have examined the lightning and rainfall and hail fall evolution (using CSU-CHILL multiparameter radar observations) of the July 10 and 12 cases in relationship to storm structure. DeCaria et al. [2000] have examined the very early, nonintense phase of the July 12 case using the Goddard 2-D cumulus ensemble model. Defer et al. (submitted manuscript, 1999) reported results on CG lightning using the interferometer and a comparison with NLDN measurements. Other investigations under way include (1) the overall impact of STERAO storms on NO_X in the upper troposphere from combined effects of transport and lightning; (2) the importance of soluble species and aqueous chemistry on the distribution of odd nitrogen species, peroxides, and formaldehyde, all of which influence subsequent ozone concentrations downwind: (3) three-dimensional calculations of photolysis frequencies of NO_2 and ozone in and around the July 10 storm; (4) the use of hydrocarbons and other tracers to examine convective transport regionally in NE Colorado during STERAO; and (5) evaluation of microphysical parameterizations in cloud models using Citation in situ microphysical observations in combination with the CSU-CHILL multiparameter radar measurements. Thus there is a diverse collection of ongoing

and potential future studies that can be undertaken using this excellent data set.

Appendix A: Description of the Carbon Monoxide Instrument Flown on the Citation

The CO instrument flown on the Citation during STERAO was a highly modified commercial IR absorption instrument (TEI model 48S) with gold-plated absorption cell and specially selected detector. The modifications included (1) mass flow was controlled with a delivery of 1.7 standard liter per minute of sample air through the absorption cell of volume 580 cm^3; (2) pressure of sample air exiting the absorption cell was controlled to constant 760 torr; and (3) temperature of the absorption cell was kept constant at 40 ± 0.2°C. Owing to limited pumping power, the instrument's response time could not be less than 20 s. Water vapor was removed from the gas sample upstream of the instrument by a dry-ice-cooled water trap. A dynamic zero baseline of the instrument was frequently determined in flight by sending the sample air through a 0.5% Pd on Al catalytic bed heated to 190 ± 0.5°C. The sensitivity of the instrument to CO was determined by standard addition and dilution of calibration gas of known CO mixing ratio (103.5 ppmv, kindly provided by D. Parrish and J. Holloway of the NOAA Aeronomy Lab) into the sample airflow. These calibrations were performed routinely at the ground before and/or after flights and on board in flight. Normally, the in-flight calibrations were used to calculate CO mixing ratios.

The intercomparison flights showed the CO measured on the Citation was on average 17% higher than the values measured on the WP3D. We chose to reduce the Citation CO data by 17% for all days to bring the archived data set of the Citation and WP3D as a whole into agreement. This decision was made because the WP3D instrument has a longer history of performance than the instrument flown on the Citation and because the instrument on the Citation was put together carefully, but quickly, for the STERAO project without a lot of opportunity for thorough evaluation. The CO measurement system of the WP3D subsequently has been intercompared with a tunable diode laser absorption system and another VUV fluorescence system of substantially different design; excellent agreement was found between all three instruments.

For the July 10 Citation measurements the on-board sensitivity calibrations used to convert raw signal to CO mixing ratio were much higher than the sensitivity calibrations of all other days. However, the ground calibrations were consistent with the ground and in-flight calibrations for other days. Also when the in-flight sensitivity calibrations were used to calculate CO from the Citation, a comparison of ascent and descent profiles for July 10 between the two aircraft showed the Citation CO data to be a factor of approximately 1.20 higher than the WP3D. This factor is comparable to the difference in sensitivity coefficient between the in-flight calibrations for July 10 and the ground calibrations and the calibrations for other days, suggesting that the actual instrument sensitivity in flight had not changed. Thus an overall correction factor of 1.40 (1.17 x 1.20) has been applied to the raw Citation CO data for the July 10 measurements presented herein.

Appendix B: Lightning Morphology and the ONERA Lightning Interferometer Measurements

Before discussing the operation of the interferometer, it is important to understand the morphology of a lightning discharge. The channel of a lightning flash is thought to spread from the initiation point (normally inside cloud) through the propagation of branched bidirectional leaders [*Mazur*, 1989]. The positive leader moves in the direction of the electric field, while the negative leader moves in the opposite direction. For negative CG flashes a negative stepped leader propagates through cloud and then steps toward the ground. This can take 100 ms or more for horizontally extensive flashes. As the negative stepped leader approaches the ground, a positive leader starts upward, makes connection to the negative leader, and initiates the short-duration (tens of microseconds), high-current return stroke which flows through the previously ionized channel. The high current of return strokes generates a strong magnetic field that is what is detected by the NLDN for both negative and positive flashes. After leader propagation, high-current discharges called K streamers or recoil streamers appear in part of the intracloud leader paths. There can be several streamers for an individual flash, and they can traverse several kilometers with total path lengths well in excess of 10 km and durations of 10 to >100 μs. Dart leaders are similar to recoil streamers, but move toward the ground following the path of the stepped leader and can initiate additional return strokes. (See *Shao et al.* [1995] for more detailed discussion.) Similar processes, but with opposite signs, are thought to occur for positive flashes, but less is known about positive CG flashes [*Shao et al.*, 1999]. Normally, there is only one return stroke, and the peak currents are frequently higher. For normal intracloud (IC) flashes a negative leader usually moves upward from the initiation point and then spreads horizontally into the regions of positive charge in the upper part of the cloud. Concurrently, positive leaders move from the initiation point into regions of negative charge at midcloud levels. Recoil streamers then move back along both the upper and lower paths created by the leaders [*Shao and Krehbiel*, 1996]. All of these components of CG and IC flashes are thought to produce NO_X with varying efficiencies [*Chameides*, 1986; *Coppens et al.*, 1998].

Because of their discontinuous propagation, the negative stepped leaders emit a lot of VHF radiation for tens to hundreds of milliseconds. Recoil streamers and dart leaders also emit a lot of VHF radiation, but for shorter periods of time. Positive leaders, because they tend to propagate continuously, do not radiate significantly, but their path can be partially inferred from the location of the recoil streamers. Negative return strokes emit VHF radiation, but have a short duration and hence are harder to detect. Positive flashes emit very little, if any, VHF radiation [*Shao et al.*, 1999].

The ONERA interferometer detects VHF radiation at a frequency of 114 MHz in a 1 MHz band with a 23 μs average of the analog signal for the 3-D recorded data and 100 μs for the real-time data. It utilizes two remote stations, which for STERAO were separated by approximately 40

km and located near Grover and south of Briggsdale, Colorado. Each station has an antenna array for determining the horizontal direction to individual VHF radiation sources by measuring phase differences. The array for determining the elevation of each source was located at the Grover site. When the amplitude of sources is greater than a preset threshold, sources are detected and recorded with a resolution of 0.25° and 0.5°in the horizontal and vertical, respectively. Based on the intersection of the direction from the two stations, the 3-D positions of the individual sources can be reconstructed. The location algorithm verifies that the reconstructed position is consistent with the source arrival times at each station.

The map in Figure 1 shows the zone inside two lobes where the placement accuracy is 2 km or better based on angular resolution of the intersecting directions and range. This is for an idealized case in which the VHF sources have sufficient amplitude such that they can be well resolved. In actual practice some of the detected VHF sources are close to the signal-to-noise level of the system. This is especially true for distant sources. When the flashes are near the edge of the lobes and close to the baseline, the sources are much closer to one station than the other. Consequently, the fixed angular resolution, which is the same for both stations, gives a larger uncertainty of distance along the tangent arc for the farther station and a scatter of sources in a quasi-radial from the closest station. We refer to this as radial dispersion. This is a classic problem for direction-finding systems and has been described by *Stanfield* [1947] and others. This source of error is difficult to quantify, but examples shown in Figure 7 suggest that the spread is substantial when the sources are near the northern or southern part of the two lobes. For individual VHF sources the *x,y,z* position uncertainty is a function of the strength of the VHF emission as well as location within the lobe. A quantitative estimate of uncertainty can be made based upon the measurement of the standard deviation of positions determined for a known emission at fixed locations [*Stanfield*, 1947]. But this has not yet been accomplished with this interferometer. For VHF sources associated with the southeastern cells of Plate 1, we estimate uncertainties for *x,y* positions of 1 – 2 km. The uncertainty increases to >10 km along the radials from the Grover site when the sources are very near the lobe boundaries (especially for weak sources), such as the most northwestern cells of the July 10 storm.

As operated for STERAO the elevation sensor of the system can determine the elevation angles of sources between roughly 8° and 48° with best sensitivity near 22.5°. For sources at 20, 40, and 60 km ranges, the lower limits for altitude determination would be 2.8, 5.6, and 8.4 km agl (4.3, 7.1, 9.9 km msl). Therefore the best 3-D reconstructions are obtained when the storms are less than 20 to 30 km from the Grover station. Cloud bases of severe storms in NE Colorado are typically 2.5 to 3.5 km agl and many of the storms investigated were more than 30 km from Grover. Consequently, altitude determinations of sources from the middle and lower part of the storms are not optimum, except for storms very close to Grover.

Data from the interferometer is in the form of VHF source locations from which individual flashes must be identified. This was done using software developed by ONERA, with some modifications suggested by NCAR. It uses the following criteria, which are based on the multiyear experience that ONERA has in working with lightning measurements from this interferometer and a predecessor with 1.6 μs time resolution [*Richard et al.*, 1986]: (1) The maximum duration of a flash is one 1s. (2) two successive points in a flash are separated by not more than 25 km. (3) The velocity between two consecutive sources must not exceed 1 x 10^8 m s^{-1}. (4). The maximum temporal gap between two sources of a flash is 250 ms. After the VHF sources are classified into individual flashes, the *x*, *y* and *z* locations of all sources for each flash can be averaged to determine a mean geometric position (*X*,*Y*, and *Z*) for the flash, but as noted above, the altitude determination is not reliable except for flashes within ~20 km of Grover.

Acknowledgments.

Many organizations and individuals have contributed to the success of the STERAO project, and we greatly appreciation their efforts. In particular, we would like to thank the NASA Atmospheric Effects of Aviation Program and R. Friedl, the NOAA Aeronomy Lab Director's Reserve, and the NCAR Director's Reserve for field support for the interferometer; the NOAA Global Change Program for partial support for B.A.R., W.C.S. and M.V. and the analysis effort; P. Kennedy, D. Brunkow, and B. Bowie of the CSU-CHILL facility both for radar support and for locating sites and assembly of the interferometer antennae; D. Breed for help with interferometer evaluation; all investigators on the NOAA WP3D and the AOC flight crews; flight crews of the UND Citation; D. Blanchard, E. Rasmussen, and E. Szoke for forecasting help, NOAA FSL for use of their facilities, J. Bresch for running the MM5 model; J. Scala and K. Pickering for running the Goddard cumulus ensemble model; and A. Seimon for permission to use his excellent photograph of the storm. The UND Citation effort was supported under National Science Foundation (NSF) grant 9634125. The CSU-CHILL National Radar Facility is supported by NSF and Colorado State University. The National Center for Atmospheric Research is partially supported by the National Science Foundation.

References

Chameides, W. L., The role of lightning in the chemistry of the atmosphere, in *The Earth's Electrical Environment*, pp. 70-77, Natl. Acad. Press, Washington, D.C., 1986.

Coppens, F., R. Berton, A. Bondiou-Clergerie, and I. Gallimberti, Theoretical estimate of NO_X production in lightning corona, *J. Geophys. Res., 103*, 10,769-10,785, 1998.

Cummins, K. L., M. J. Murphy, E. A. Bardo, W. L. Hiscox, R. B. Pyle, and A. E. Pifer, A combined TOA/MDF technology upgrade of the U.S. National Lightning Detection Network, *J. Geophys. Res., 103*, 9035-9044, 1998.

Decaria, A., et al. A cloud-scale model study of lightning generated NO_X in an individual thunderstorm during STERAO-A, *J. Geophys. Res., in press*, 2000.

Dickerson, R. R., et al. Thunderstorms: An important mechanism in the transport of air pollutants, *Science, 235*, 460-465, 1987.

Doviak, R. J., and D. S. Zrnic, *Doppler radar and weather observations*, 2nd ed. 562pp., Academic, San Diego, Calif. 1993.

Fankhauser, J. C., and C. Wade, The environment of the storms, in *Hailstorms of the Central High Plains*, vol. 1, edited by C.A. Knight and P. Squires, pp. 5-33, chap 2, Colo. Assoc. Univ. Press, Boulder, 1982.

Frost, G. F., et al., Photochemical ozone production in the rural southeastern United States during the 1990 Rural Oxidants in the Southern Environment (ROSE) program, *J. Geophys. Res., 103*, 22,491-22,508, 1998.

Holden, D. N., C. P. Munson, and J. C. Devenport, Satellite observations of transionospheric pulse pairs, *Geophys. Res. Lett., 22*, 889-892, 1995.

Huntrieser, H., H. Schlager, C. Feigl, and H. Holler, Transport and production of NO_X in electrified thunderstorms: Survey of previous studies and new observations at midlatitudes, *J. Geophys. Res., 103*, 28,247-28,264, 1998.

Jorgensen, D. P., T. Matejka, and J. D. DuGranrut, Multi-beam techniques for deriving wind fields from airborne Doppler radars, *Meteorol. Atmos. Phys., 59*, 83 – 104, 1996.

Krehbiel, P. R., The electrical structure of thunderstorms, in *The Earth's Electrical Environment*, pp. 90-113, Natl. Acad. Press, Washington, D.C., 1986.

Krehbiel, P. R., R. Thomas, and W. Rison, Lightning mapping observations during MEaPRS in central Oklahoma, *Eos, Trans. AGU, 79* (45), Fall Meet Suppl., F127, 1998.

Lang, T., Relationship between storm structure and lightning activity in Colorado convection observed during STERAO-A, masters thesis, Colo. Univ., Fort Collins, 1997.

Lang, T. J., S. A. Rutledge, J. E. Dye, M. Venticinque, P. Laroche, and E. Defer, Anomalously low negative cloud-to-ground flash rates in intense convective storms observed during STERAO-A, *Mon. Weather Rev., 128*,160-173, 2000.

Laroche, P., A. Bondiou, P. Blanchet, J. Pigere, M. Weber, and B. Boldi, 3D mapping of lightning discharge within storms, paper presented at International Aerospace and Ground Conference on Lightning and Static Electricity, Mannheim, Germany, 1994.

Lhermitte, R. and P.R. Krehbiel, Doppler radar and radio observations of thunderstorms, *IEEE Trans. Geosci. Electron., GE-17*(4), 161-171, 1979.

Lhermitte, R., and E. Williams, Cloud electrification, *Rev. Geophys, 21*, 984-992, 1983.

Madronich, S., Photodissociation in the atmosphere, 1, Actinic flux and the effects of ground reflections and clouds, *J. Geophys. Res., 92*, 9740-9752, 1987.

Maier, L., C. Lennon, P. Krebhiel, and, M. Maier, Lightning as observed by a four-dimensional lightning location system at Kennedy Space Center, paper presented at 10th International Conference on Atmospheric Electricity, International commission on Atmospheric Electricity, Osaka, Japan, 1996.

Matejka, T. and D.L. Bartels, The accuracy of vertical air velocities from Doppler radar data, *Mon. Weather Rev., 126*, 92-117, 1998.

Mazur, V., Triggered lightning strikes to aircraft and natural intracloud discharges, *J. Geophys. Res., 94*, 3311-3325, 1989.

Mohr, C.G., L.J. Miller, R.L.Vaughan, and H.W. Frank, The merger of mesoscale data sets into a common Cartesian format for efficient and systematic analyses, *J. Atmos. Oceanic Technol., 3*, 144-161, 1986.

Noxon, J. F., Atmospheric nitrogen fixation by lightning, *Geophys. Res. Lett., 3*, 463-465, 1976.

O'Brien, J.J., Alternative solutions to the classical vertical velocity problem. *J. Appl. Meteorol., 9*, 197-203, 1970.

Orville, R. E., Spectrum of the lightning stepped leader, *J. Geophys. Res., 73*, 6999-7008, 1968.

Orville, R. E., Spectrum of the lightning dart leader, *J. Atmos. Sci., 32*, 1829-1837, 1975.

Pickering, K.E., Y. Wang, W.-K. Tao, C. Price and J. P. Muller, Vertical distributions of lightning NO_X for use in regional and global chemical transport models, *J. Geophys. Res., 103*, 31,203-31,216, 1998.

Poulida, O., R.R. Dickerson, and A. Heymsfield, Stratosphere-troposphere exchange in a midlatitude mesoscale convective complex, 1; Observations, *J. Geophys. Res., 101*, 6823-6836, 1996.

Price, C., J. Penner. and M. Prather, NO_X from lightning, 1, Global distribution based on lightning physics, *J. Geophys. Res., 102*, 5929-5941, 1997.

Proctor, D. E., Regions where lightning flashes began, *J. Geophys. Res., 96*, 5099-5112, 1991.

Ray, P.S., D.R. MacGorman, W.D. Rust, W.L. Taylor, and L.W. Rasmussen, Lightning location relative to storm structure in a supercell storm and a multicell storm, *J. Geophys. Res., 92*, 5713-5724, 1987.

Richard, P., A. Delannoy, G. Labaune, and P. Laroche, Results of spatial and temporal characterization of the VHF-UHF radiation of lightning, *J. Geophys. Res., 91*, 1248-1260, 1986.

Ridley, B. A., J. E. Dye, J. G. Walega, J. Zheng, F. E. Grahek, and W. Rison, On the production of active nitrogen by thunderstorms over New Mexico, *J. Geophys. Res., 101*, 20,985-21,005, 1996.

Rust, W. D., Utilization of a mobile laboratory for storm electricity measurements, *J. Geophys. Res., 94*, 13,305-13,311, 1989.

Rutledge, S. A., E. R. Williams, and T. E. Keenan, The down under Doppler and Electricity Experiment (DUNDEE): Overview and preliminary results, *Bull. Am. Meteorol. Soc. 73*, 3-16, 1992.

Shao, X. M., and P. R. Krehbiel, The spatial and temporal development of intracloud lightning, *J. Geophys. Res., 101*, 26,641-26,668, 1996.

Shao, X. M., P. R. Krehbiel, R. J. Thomas, and W. Rison, Radio interferometric observations of cloud-to-ground lightning phenomena in Florida, *J. Geophys. Res., 100*, 2749-2783, 1995.

Shao, X. M., C.T. Rhodes, and D.N. Holder, RF radiation observations of positive cloud-to-ground flashes, *J. Geophys. Res., 104*, 9601-9608, 1999.

Skamarock, W.C., J.G. Powers, M. Barth, J.E. Dye, T. Matjka, D. Bartels, K. Baumann, J. Stith, D.D. Parrish, and G. Hubler, Numerical simulations of the 10 July STERAO/Deep convection experiment convective system: Kinematics and transport, *J. Geophys. Res., in press*, 2000.

Smith, D. A., X. M. Shao, D. N. Holden, C. T. Rhodes, M. Brook, P. R. Krehbiel, M. Stanley, W. Rison, and R.J. Thomas, A distinct class of isolated intracloud lightning discharges and their associated radio emissions, *J. Geophys. Res., 104*, 4189-4212, 1999.

Smyth, S.B., et al., Factors influencing the upper free tropospheric distribution of reactive nitrogen over the South Atlantic during the TRACE A experiment, *J. Geophys. Res., 101*, 24,165-24,186, 1996.

Stanfield, R.G., Statistical theory of direction finding fixing, *Proc. Inst. Electr. Eng., 94*, 762-770, 1947.

Stith, J., J. E. Dye, B. Ridley, P. Laroche, E. Defer, K. Baumann, G. Hubler, R. Zerr, and M. Venticinque, NO_X signatures from lightning flashes, *J. Geophys. Res., 104*, 16,081-16,089, 1999.

Willett, J. C., J. C. Bailey, and E. P. Krider, A class of unusual lightning electric field waveforms with very strong high-frequency radiation, *J. Geophys. Res., 94*, 16,255-16,267, 1989.

Williams, E. R., B. Boldi, A. Matlin, M. Weber, S. Hodanish, D. Sharp, S. Goodman, R. Raghavan, and D. Buechler, The behavior of total lightning activity in severe Florida thunderstorms, *Atmos. Res., 51*, 245-265, 1999.

D. Bartels and T. Matejka, NOAA National Severe Storms Laboratory, 325 Broadway, Boulder, CO 80303.

M. Barth, J.E. Dye, B.A. Ridley, W. Skamarock, and M. Venticinque, National Center for Atmospheric Research, P.O. Box 3000, Boulder, CO 80307. (dye@ucar.edu)

P. Blanchet, E. Defer, P. Laroche, and C. Thery, Office Nationale d'Etudes.

K. Baumann, Georgia Institute of Technology, 221 Bobby Dodd Way, Atlanta, GA 30332.

F.C. Fehsenfeld, G. Frost, J.S. Holloway, G. Hubler, D.D. Parrish, T. Ryerson, M. Trainer, and A. Tuck, NOAA Aeronomy Laboratory, 325 Broadway, Boulder, CO 80303.

T. Lang and S.A. Rutledge, Colorado State University, Port Collins, CO 80523.

J. Stith and R. Zerr, University of North Dakota, Grand Forks, ND 58202.

(Received February 5, 1999; revised July 19, 1999; accepted July 28, 1999.)